Modelling burnt-bridge ratchets; optimizing their efficiency and motility

by

Mark Rempel

B.Ed., University of the Fraser Valley, 2018
B.Sc., University of the Fraser Valley, 2016

Thesis Submitted in Partial Fulfillment of the
Requirements for the Degree of
Master of Science

in the
Department of Physics
Faculty of Science

© Mark Rempel 2022
SIMON FRASER UNIVERSITY
Summer 2022

Copyright in this work is held by the author. Please ensure that any reproduction or re-use is done in accordance with the relevant national copyright legislation.

Declaration of Committee

Name:	**Mark Rempel**
Degree:	**Master of Science**
Thesis title:	**Modelling burnt-bridge ratchets; optimizing their efficiency and motility**
Committee:	**Chair:** Malcolm Kennett Associate Professor, Physics
	Eldon Emberly Supervisor Professor, Physics
	Nancy Forde Committee Member Professor, Physics
	David Sivak Examiner Associate Professor, Physics

Abstract

Molecular motors carry out tasks at scales, speeds and efficiencies largely unattainable for conventional motors. A class of molecular motors known as burnt-bridge ratchets (BBRs) are found all throughout biology, providing key functions such as the movement and organization of biomolecular cargo. The motion and operation of these motors are well characterized, however the efficiencies have not yet been fully elucidated. In this thesis I provide an overview of the characteristics of molecular motors, their physical properties and key metrics as well as review notable synthesized BBRs. I then detail several models of BBRs to characterize their motility and efficiency. In each of these models I run computational simulations to map out the parameter space and determine regions of optimal efficiency and motility. These models provide insights and experimentally testable predictions which can provide guidance for the optimization of synthetic molecular motors.

Keywords: molecular motor; burnt-bridge ratchet; efficiency; computational model

Dedication

To Leo, may you always find beauty and inspiration as you explore this world.

Acknowledgements

I thank Eldon for his kindness, patience and guidance over these past two years. He was more than willing to be flexible amidst his busy life and to provide advice and support after hours. He has set the bar high for the kind of teacher that I strive to be.

I would like to thank Nancy for her advice, insights and willingness to supervise my graduate work. I have enjoyed the thoughtful and sincere conversations we had.

I am grateful for my family, particularly my wife, Rachel, who provided immeasurable support and encouragement through this process. And to Leo, your exuberance for life and your love to learn helped me also find joy in my learning.

Table of Contents

Declaration of Committee ii

Abstract iii

Dedication iv

Acknowledgements v

Table of Contents vi

List of Tables viii

List of Figures ix

1 Introduction 1

1.1 Molecular Motors . . . 3

1.1.1 Processivity . . . 3

1.1.2 Directionality . . . 4

1.1.3 Autonomy . . . 4

1.1.4 Stall force . . . 4

1.1.5 Molecular motors vs. conventional motors . . . 5

1.1.6 Efficiency . . . 7

1.1.7 Maxwell's Demon . . . 8

1.2 Burnt-Bridge Ratchets . . . 10

1.3 Synthetic Molecular Motors . . . 15

1.4 Thesis organisation . . . 20

2 Optimizing efficiency and motility of a polyvalent molecular motor 22

2.1 Introduction . . . 22

2.2 Materials and Methods . . . 23

2.2.1 Force-Dependent Unbinding . . . 27

2.2.2 Efficiency . . . 29

2.3 Results . . . 29

2.4 Discussion . . . 39
2.5 Appendix . . . 40
2.5.1 Analytic approximation . . . 40
2.5.2 Steady-state concentration . . . 43
2.5.3 Consumption rate scaling when rebinding is included . . . 44

3 Characterising efficiency and motility of a diffusing polyvalent motor hub 45
3.1 Introduction . . . 45
3.2 Model and methods . . . 46
3.2.1 Efficiency . . . 48
3.3 Results . . . 49
3.4 Discussion . . . 55

4 Conclusions and Future Work 58
4.1 Future work . . . 59
4.1.1 Model . . . 59
4.1.2 Efficiency . . . 62
4.1.3 Preliminary results . . . 62
4.1.4 Summary . . . 62

Bibliography 65

List of Tables

Table 2.1 Characteristic quantities 26
Table 2.2 Model variables 28

List of Figures

Figure 1.1 Model free energy landscape of a kinesin motor. 6
Figure 1.2 A BBR ratcheting high energy flutuations 10
Figure 1.3 Summary of processive Chintase reaction cycle. 13
Figure 1.4 Plasmid segregation via BBR mechanism. 14
Figure 1.5 BBR model of influenza. 15
Figure 1.6 Synthetic rotor schematic. 16
Figure 1.7 Sample trajectories of P1 plasmids over a DNA susbtrate. 17
Figure 1.8 Schematic of DNA walker locomotion. 18
Figure 1.9 Depiction of the polyvalent DNA motor. 19

Figure 2.1 Deterministic model schematic. 24
Figure 2.2 Time dependence of hub velocity and substrate consumption rate. . 31
Figure 2.3 Dependence of velocity and consumption rate on system parameters. 33
Figure 2.4 Dependence of efficiency on system parameters 35
Figure 2.5 Effects of rebinding on efficiency. 37
Figure 2.6 Effects of complex unbinding on efficiency. 38
Figure 2.7 Comparison of analytic and numerical velocities and efficiencies . . 42
Figure 2.8 Consumption rate approximation. 43
Figure 2.9 Velocity scaling with consumption rate 44

Figure 3.1 Stochastic model schematic 47
Figure 3.2 Motor dynamics and reaching steady-state. 50
Figure 3.3 MSD for different diffusion constants 51
Figure 3.4 Motor properties in D'/v' parameter space. 52
Figure 3.5 Bound complex concentration for diffusive and ballistic regions. . . 53
Figure 3.6 Motor properties in a_{tot}/v' parameter space. 54
Figure 3.7 Velocity and characteristic motion time dependence. 56

Figure 4.1 Finite hub model schematic. 60
Figure 4.2 Effect of size and availability on $B_h(\phi, \tau)$. 63
Figure 4.3 Effect of hub size on efficiency. 63

Chapter 1

Introduction

Machines allow for the completion of difficult tasks; it is this property that correlates the advances in machine technology to the greatest societal changes in history. The earliest machines made the transfer of manually generated mechanical energy from one object to another more efficient, such as the use of a wheel or lever. Eventually, mechanical energy from the environment, such as water flow or wind, was harnessed to accomplish greater energy demanding tasks. However, it was the conversion of chemical energy to mechanical work that ultimately brought about the greatest advances.

In the 1700s a revolutionary invention was taking Europe by storm. A new machine was able to use stored chemical energy in fossil fuels to create a heat gradient that would produce useful work. With vast landmark improvements by Thomas Newcomen and James Watt, the steam engine was becoming a powerful tool that spurred on the industrial revolution and permanently altered any society touched by it [1]. It took many contributions and advances to progress from the most rudimentary steam engines in 1606 until 1760 in which they were produced on an industrial scale. The most notable advances include those that improved the power and efficiency of the motor, as these improvements allowed the engine to be viable and cost-effective in many settings.

Two centuries later began a modern revolution of engines on a much smaller scale but no less important. In his legendary 1959 lecture, "There's plenty of room at the bottom", Richard Feynman expressed his expectation and encouragement of future advances in micro and even nano-scaled operations [2]. In an attempt to encourage advances in this field he offered $1000 to whomever could construct a motor of less than 1/64 inch cubed. While the challenge was quickly satisfied by non-novel methods, this gentle push on the scientific community may have been the catalyst to help realize the future of nanotechnology [3].

At this point there was already some understanding that molecular sized motors existed in the body. In fact, in 1864 Wilhelm Kunhe correctly predicted that a single protein, which he called myosin, was responsible for the contraction of muscles [4]. But it was not for another 80 years that anyone had any rigorous understanding of myosin. In 1939, Engelhardt and Ljubimowa showed that myosin acted as an ATPase, consuming what was believed to be

the energy source of muscle contraction [5]. Later, Szentz-Georgi showed that a new thread-like polymer, known as actin, when in the presence of myosin and ATP, acted similarly to contracting muscle tissue[6]. However, it was not until well after Feynmann's famous lecture that myosin was well understood and characterised as a self propelling, autonomous molecular motor [7].

The discovery of dynein in 1965 and kinesin in 1985 further revealed the capabilities of molecular motors in carrying out diverse tasks at the molecular scale [8, 9]. Myosin, dynein and kinesin make up the family of motors known today as the cytoskeletal motors. These motors utilize a cycle consisting of several conformational changes induced by binding and catalyzing ATP. During this cycle, a power stroke step occurs leading to net forward motion and the output of work. The power stroke step is the source of mechanical energy that drives motion. The observations of these motors provided insights into how molecular motors operate, but it was not until much later that the first breakthroughs in synthetic motors were achieved.

The realization that biological motors of this scale were possible, and in fact abundant in nature, inspired efforts to synthesize molecular motors. However, progress was slow and small steps were taken to create components of motors rather than the entire mechanism. Notably, in 1999 Kelly et al. synthesized the first molecular ratchet-and-pawl mechanism [10]. While unidirectional motion was achieved, they were unable to continue the motion for longer than the first step. In a related study, Koumura et al. created a molecular motor that was able to move in continual unidirectional rotation via light stimulated cis-trans isomerizations [11]. The first synthetic molecular motors mainly used a bottom-up approach in which chemical compounds were synthesized to create novel mechanisms [12].

While the bottom-up approach led to ground-breaking developments, these motors were either incomplete or severely limited in their operation. Instead, a top-down approach in which known biological mechanisms are either reconstituted or emulated would provide greater promise. A mechanism known as a burnt-bridge ratchet (BBR) was an ideal candidate due to its relative simplicity and versatility [13, 14]. Saffarian et al. found that a group of enzymes known as matrix metalloproteases (MMPs) processively travel over collagen in a manner characterised by a BBR mechanism [15]. MMP is able to persistently move across the extracellular matrix by attaching to and cutting collagen fibrils. In this way, an asymmetry of bindable substrate was established that rectified the fluctuations of the enzyme and biased its motion.

Chemical gradients are used to establish patterns and motion all throughout nature [16, 17, 18]. BBRs generate these gradients spontaneously to rectify their motion and one of the most well studied systems is the two-protein (ParABS) system that segregates genetic information in bacteria. Vechiarelli et al. proposed a BBR type mechanism, known as a diffusion ratchet mechanism, that segregates plasmids by facilitating the interaction of nucleoid-bound ParA to plasmid-bound ParB. ParB binds ParA and then catalyzes the

dissociation of ParA from the nucleoid; this generates the gradient necessary for sustained motion [19, 20, 21]. Since then, additional work has been done to reconstitute BBRs in vitro, to further understand them and improve their design as viable and effective synthetic motors. Recent studies have shown synthetic BBR motors are able to carry out rapid, persistent motion and have demonstrated the wide range of operations that in vivo BBRs carry out at the sub-cellular scale [22, 23, 24, 25, 26].

From the first steam engine to synthetic molecular motors, every machine is governed by the basic principles of energy conversion. Free energy of one kind is converted to mechanical work. The second law of thermodynamics dictates that during this conversion some free energy is lost due to an increase in entropy, however, the amount that is lost varies from system to system. The ability to convert this energy to mechanical motion efficiently has been the key to making motor technology viable and has led to industry shaping advances. It is with the focus of characterising and understanding the efficiency of molecular motors that this thesis is written.

This Introduction is organized into three sections. First I overview molecular motors, their physical properties and how they operate. Then I look at the burnt-bridge ratchets, the underlying physics of their operation, their key characteristics and the models that have been developed to understand them. In particular, I outline various definitions of efficiencies, detail methods for determining efficiencies for biological systems and provide benchmark values from well studied motors. Lastly, I review some of the synthetic reconstitutions of several kinds of molecular motors with an emphasis on the BBRs.

1.1 Molecular Motors

One may categorize molecular motors into two classes: rotary and linear. Rotary motors spin on a central axis, with common examples being bacterial flagellum motor and F1-ATPase [27, 28]. There are many more linear motors such as the cytoskeletal motors of myosin, kinesin and dynein and the enzymatic motors of collagenase, helicase, chitinase and cellulase [29]. Most linear motors "walk" along tracks of enzyme-specific polymers such as microtubules and are able to support a wide range of tasks by providing transport of cargo over large distances. Several characteristics describe the physical nature of molecular motors: processivity, directionality, autonomy, stalling force and efficiency.

1.1.1 Processivity

Processivity describes a motor's ability to remain attached to its substrate and carry out chemical reactions [30]. Both kinesin and dynein keep at least one leg on the track and so are highly processive; they are able to travel several hundred nanometers in a single trajectory [31, 32]. Some myosins on the other hand, frequently come off the track as part of the motor cycle and must make up for the lack of processivity by employing an ensemble of

many myosin motors working together. As long as enough myosins remain attached to the cargo at a given time, the ensemble may collectively stay connected and work processively [33]. In the early years of engineering synthetic molecular motors, motor processivity was difficult. Many motors demonstrated motion for just a handful of steps before the system stalled [11, 34].

1.1.2 Directionality

Directionality describes a motor's preference to walk one way over another. Directionality is essential for many kinesins and dyneins as their cargo must reach specific destinations and the entire ensemble of kinesins or dyneins must favor movement along one direction of a microtubule. The directionality of kinesins and dyneins is related to the polarity of the microtubule which ultimately alters the free energy landscape of the motor. This free energy landscape may be modeled by something similar to a sawtooth ratchet which forces the entire ensemble to energetically favor one direction along a microtubule [35, 36]. For other motors directionality is unnecessary, such as the HA-NA system found on the influenza virus, which allows the viral capsid to explore a greater area simply by moving along any path that is self-avoiding [26]. In this case any movement is beneficial, so directionality is not important.

1.1.3 Autonomy

Autonomy describes a motor's ability to operate without the intervention of an external agent. Of course, many in vivo motors operate autonomously, carrying out necessary operations within the same environmental conditions or, when environmental change is required, may autonomously alter its surroundings. However, autonomy has been difficult to achieve in synthetic molecular motors. Many motors such as the acid-base shuttles or the light/thermal stimulated trans-cis rotors required constant environmental changes to generate persistent motion [11, 37]. Since the first synthetic motors this problem has been largely solved; now a wide variety of synthetic motors can function without any external intervention [24, 38, 39].

1.1.4 Stall force

The stall force of a motor describes the mean maximum load that a motor may carry. The stall force characterises which tasks are feasible for a given number of motors. Kinesin and myosin stall at around 7 and 5 pN respectively, and this is enough for these motors to drag micron-sized cargo through a viscous environment [40, 41, 42]. Remarkably, a study by Blanchard et al. demonstrated that a synthetic DNA-RNA based BBR may persist through resisitive forces of around 150 pN [43]. This showed that molecular motors may be designed to accomplish tasks spanning a wide variety of loads.

1.1.5 Molecular motors vs. conventional motors

In some ways, molecular motors operate the same as the conventional motors of steam, diesel and gas. Molecular motors consume chemical energy with the goal of accomplishing some mechanical work. Just as with conventional motors, the process of energy conversion leads to a change in entropy that is greater than or equal to zero; this is known as the 2nd law of thermodynamics. It then follows that the energy put into a system must be of lower entropy than the energy that is output [44]. The free energy (or energy able to be converted to work) in a system follows $\Delta F = \Delta U - T\Delta S$, where ΔU is the change in internal energy, T is the temperature of the system and ΔS is the change in entropy [45]. So the amount of useful energy decreases during an energy conversion process. Therefore, motors must make use of some form of energy that is low in entropy. The typical energy source for molecular motors, adenosine triphosphate (ATP), releases roughly 31 kJ/mol of free energy during its conversion to adenosine diphosphate (ADP) with roughly 28 kJ/mol of this free energy resulting from an internal energy change and 3 kJ/mol resulting from an increase in entropy [46]. This low entropy fuel is converted to mechanical motion which is eventually dissipated by friction and viscous drag as heat.

Like heat engines, many molecular motors operate on a cycle. They make conformational changes at each stage in their cycle until returning to the initial state [44]. As opposed to one-shot motors, which undergo an irreversible conformation change in the motor and are incapable of returning to their initial state, cyclic motors may generate small amounts of work repeatedly, culminating in the completion of large energy demanding tasks. Cyclic motors need only a constant supply of fuel during each step, and in the case of molecular motors this fuel may be recycled. Perhaps not surprisingly however, molecular motors have less in common with conventional motors than might be suggested by their name.

Unlike heat engines, molecular motors operate entirely in a single bath of some mean thermal energy. This means that energy cannot be used to generate a temperature gradient as in conventional heat engines. Instead, chemical energy must be directly converted to motion. This may be done by altering the free energy landscape as a result of a chemical reaction [47]. A free energy landscape change may result from a conformation change in the motor, as is seen in the relative "head" and "leg" motions of myosin and kinesin, or an irreversible surface change as is seen in enzymatic motors. These conformation and surface changes make it energetically favorable for the motor to step unidirectionally. Figure 1.1 shows the reconstruction of the free energy landscape of kinesin and describes two scenarios in which proteins alter the energy landscape and bias their motion [48]. The process of ATP binding and ATP hydrolysis (which is catalyzed by a kinesin binding site) results in a shift of the energy landscape which allows the motor to pass through regions that would be energetically unfavorable prior to this.

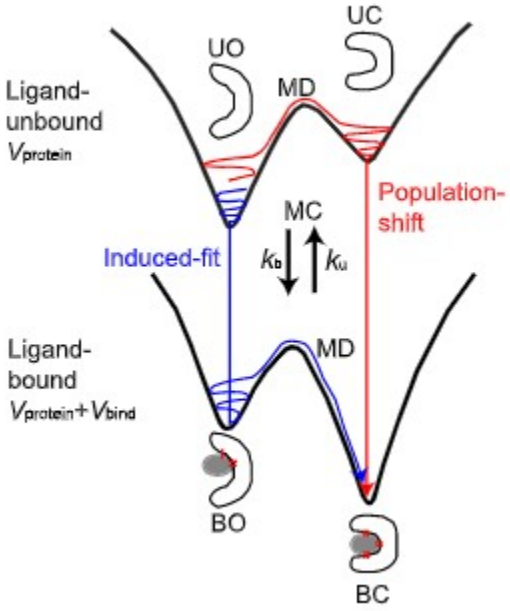

Figure 1.1: **Model free energy landscape of a kinesin motor.** In the induced-fit scenario, a protein located at the open conformer on the unbound surface (UO) binds the ligand to jump onto the bound surface (BO),which is followed by the conformational change to the closed conformation (BC). Conversely, in the population-shift scenario,the protein preexists in the closed form without ligand (UC) at some small probability and this fraction can bind the ligand directly to reach the (BC). *Credit Okazaki et al. (2008)* [48]. Images reproduced with permission from the owners.

Energy fluctuations of conventional engines are typically small compared with their energy output. However, due to the scale of molecular motors and the magnitude of their energy output, thermal fluctuations are significant [49]. Molecular motors must be able to operate persistently while under assault from random forces of a similar scale to what they generate. These forces manifest themselves as random walks or Brownian motion. The influence of random motion presents additional problems with which motors must cope. For example, directionality becomes difficult to achieve due to the tendency to follow a random walk rather than the driving force [50]. As well, the ability to stay in contact with cargo and track, processivity, becomes an important characteristic of molecular motors, as a lack in this regard may result in the motor leaving a task incomplete.

Because of their size, molecular motors operate in the low Reynolds number regime, where friction dominates [44]. This means that inertial forces are insignificant and the velocity of a motor is directly proportional to the force it may exert on its surroundings. Because of this, molecular motors require persistent driving forces for the duration of their motion. This is different from conventional heat engines that have large moving parts that must be accelerated and will continue moving for some time after the force has stopped.

1.1.6 Efficiency

Efficiency characterises the fraction of work output from a given amount of input energy. The efficiency of any motor is a vital metric that determines the viability of the motor and what tasks are feasible and cost-effective; because of this, some of the greatest advances in motor technology were punctuated by an increase in efficiency [1]. Efficiency was initially considered for the case of steam engines as a means to quantify the fuel needed to complete a task [51]. For a heat engine bound between two reservoirs, such as a steam engine, efficiency is best described by the thermodynamic efficiency, denoted as η_T. Here $\eta_T = \frac{W}{Q_h}$, where W is the work done by the system and Q_h is the heat used by the system [52]. In 1824, Carnot correctly predicted the upper bound of this efficiency for any heat engine [53]. He determined the upper bound of work done by the engine $W = Q_h + Q_c$, where Q_c is the heat released by the system. Here $Q_h = T_h \Delta S$, and $Q_c = -T_c \Delta S$, where ΔS is the entropy exchanged between the hot and cold reservoir. From this, the Carnot efficiency may be written as $\eta_c = 1 - \frac{T_c}{T_h}$, where T_c is the temperature of the cold reservoir and T_h is the temperature of the hot reservoir. The Carnot efficiency is the upper bound of the thermodynamic efficiency. Thermodynamic efficiency is well defined and bounded by one.

Since biological systems do not operate under a thermal gradient a new formulation of the efficiency is required. One may describe the efficiency of a molecular motor as the rate of free energy output of the motor divided by the rate of free energy input, $\eta = \Delta \dot{G}_{out} / \Delta \dot{G}_{in}$ [54]. However, as is the case for many in vivo systems, if the motor does not generate free energy but only works against viscous drag, this definition is not useful. Wang et

al. propose that the free energy output should be substituted with the work done by viscous drag, $\Delta\dot{G}_{out} = \langle F_d \rangle \langle v \rangle$, where $\langle F_d \rangle$ is the ensemble average drag force and $\langle v \rangle$ is the ensemble average motor velocity. In the overdamped regime $\langle F_d \rangle = \gamma \langle v \rangle$, where γ is the drag coefficient. These substitutions lead to a form of efficiency which they name the Stokes efficiency,

$$\eta_s = \frac{\langle F_d \rangle \langle v \rangle}{\Delta\dot{G}_{in}} = \frac{\gamma \langle v \rangle^2}{\Delta\dot{G}_{in}}.$$

As a benchmark specifically for kinesin, which burns one ATP molecule per 8 nm step, the efficiency is the power of viscous drag on the cargo divided by the rate of free energy released by the ATP hydrolysis reactions. Kinesin is known to move at velocities of $200 - 800\,\mathrm{nm\,s^{-1}}$ while undergoing a viscous drag force of $4 - 6$ pN, yielding a power of $800 - 4800\,\mathrm{pN\,nm\,s^{-1}}$ [55, 56, 57]. Assuming the motor does not step backwards, The consumption rate of ATP can be determined by dividing the velocity by the step length; using values from before we get $25 - 100\mathrm{s}^{-1}$. For these studies, the free energy released per ATP reaction was estimated to be $20\mathrm{k_BT}$. These values lead to an efficiency of $40 - 70\%$.

These efficiencies are reasonable and fall in line with those provided in the literature. Many molecular motors have a very high efficiency of nearly 100% for F1-ATPase and around 50% for the cytoskeletal motors [58, 59, 60]. Compare this with a standard spark ignition combustion engine that converts only 25% of its energy into useful work [61]. Due to the superior efficiency of biomotors over conventional man-made motors, the study of in vivo molecular motors provides insights into the creation of highly efficient synthetic motors. Further study and characterisation of molecular motor efficiencies will aid in this pursuit.

1.1.7 Maxwell's Demon

Bound by the 2nd law of thermodynamics, a system is only able to access the free energy from a given source. The free energy is the internal energy less an entropy dependent term. So the greater the entropy of a source, the less useful this energy is, and the smaller the energy fraction that is available to be turned into work [44]. In the past, theoretical ratchets have been proposed as thought experiments that could rectify thermal fluctuations, supposedly spontaneously reducing entropy and increasing the free energy of a system without the input of any work. In these ratchets, work is extracted by permitting high energy fluctuations to pass a barrier in one direction but not the other [62]. For example, two thermal baths may initially be at thermal equilibrium with each other but the placement of the ratchet may permit a temperature difference between the baths. The two baths may then do work as they approach equilibrium once more, thereby extracting work without the use of any apparent free energy and breaking the 2nd law of thermodynamics. This type of mechanism is know as a Maxwellian demon, named after James Maxwell who had

originally proposed it [63]. A thought experiment by Lippman suggested that a ratchet and pawl mechanism could be used as a physical Maxwellian demon, whereby random motion of particles would strike the ratchet and only those that jostled the ratchet in the favorable direction would be allowed to move the ratchet; those shifting the ratchet unfavorably would be stopped by the pawl [64]. However, a physical form of this demon was believed to be impossible simply because it violated the 2nd law of thermodynamics, one of the most rigorously observed laws in physics. However, this refutation is considered unsatisfactory due its reliance on another law and circular reasoning. One refutation for the physical existence of the demon came from Richard Feynaman, who suggested that if the ratchet and pawl were at the same temperature as the reservoir, then the pawl would undergo its own Brownian motion of equal energy fluctuations as the other particles in the system, and would frequently fail to prevent unfavorable motion [65]. He showed that this would allow motion equally as likely in either direction and would therefore produce no work. In order to generate work the ratchet and pawl would need to be at held at some other lower temperature than the reservoir so that the fail rate remained less than the forward rate [64]. Of course, the ratchet and pawl would quickly thermalize with the reservoir unless work from an external source is continually done to prevent this. So the ratchet and pawl mechanism can rectify thermal fluctuations so long as work is being done elsewhere. In other words, motors of this kind cannot make use of energy that is high in entropy without the addition of work.

While Brownian ratchets alone cannot rectify thermal fluctuations, they may do so as long as work is being done on them. For example, the operation of kinesin acts as a Brownian ratchet that locks in random motion of the leg in one direction but not the other by consuming ATP at each step [66, 67]. The hydrolyzed ATP prevents further motion of the leg until the other has moved forward a single step since the reverse reaction is energetically unfavorable. Other motors such as the enzymatic motors of chitinase and collagenase use a burnt-bridge ratchet (BBR) mechanism in which thermal fluctuations are locked in by irreversibly consuming substrate, such as a chitin or collagen polymer [15, 68]. The cleavage of a monomer at each step either completely prevents or deters the motor from back-tracking, resulting in biased forward motion. The energy that this ratchet uses comes directly from the thermal fluctuations of its environment but ultimately draws free energy from the binding energy of the polymer. The burning of free energy stored in the polymer is the added work that allows for the rectification of thermal fluctuations.

It should be noted that work may come in the form of information flow and need not result from conventional forces [69, 70]. Motors can exploit observations of fluctuations to extract work from their surroundings at the cost of increasing the entropy of the system. For example, an experimental information ratchet was created by Saha et al. in which a micron-sized bead was set in a laser trap [70]. The bead was constantly observed for fluctuations that did positive work past a predefined threshold. Once it passed a threshold

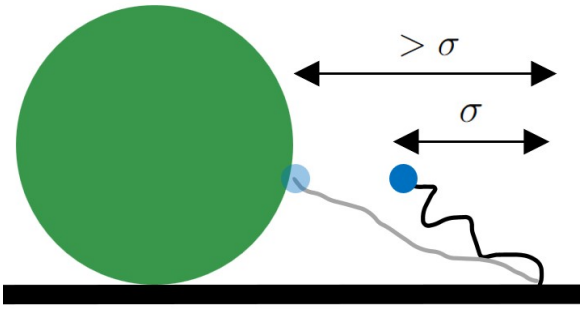

Figure 1.2: **A BBR ratcheting high energy flutuations.** The motor hub (green) ratchets high energy fluctuations ($E > 1/2k_BT$) by capturing the position of the polymer-bound substrate (blue) when it reaches a displacement of $> \sigma$.

of position the electronic monitoring system turned off the laser trap and re-positioned the trap to be in line with the new position of the bead. In this way, no work was being done to the bead but it was able to gain energy through the continual observation by the system. Brownian ratchets may also operate in a similar manner. Figure 1.2 shows a motor hub in a buffer with thermal energy, k_BT, and positioned outside the mean squared displacement, σ, of a fluctuating substrate. If the motor is able to wait at a threshold outside σ and observe the substrate as it makes a large enough fluctuation it may extract greater than the mean thermal energy from the substrate by binding to the substrate and being repositioned to the polymer's equilibrium position. Since the mean free energy of a polymer fluctuating in a thermal bath can be approximated by a harmonic potential well, $E = 1/2k\sigma^2 = 1/2k_BT$, a stretch of $> \sigma$ leads to an energy of $> 1/2k_BT$ [71]. However, in order to make this observation and repeat the cycle with the next substrate molecule, the motor must catalyse the dissociation of the substrate. This ratcheting of high energy thermal flutuations allows for the hub to potentially extract energy without doing work in a similar manner to the system presented by Saha et al. The next section will discuss BBRs in more detail and overview the main models that have been used to understand them.

1.2 Burnt-Bridge Ratchets

Burnt-bridge ratchet motors typically consist of substrate binding and an enzymatic reaction that catalyzes the removal/destruction of the substrate. Such a motor binds to substrate that is bound to some track (or is itself the track, e.g. collagen) and then catalyses the dissociation of a portion of the substrate, making an effectively irreversible change to its environment. Once a substrate has been removed from the track, the motor can no longer interact with it. This process leads to a gradient of interactive substrate that biases the motion of the motor in the direction of the gradient [72, 73, 74]. In the case of chitinase, the motor takes random walks along the chitin polymer and sequentially cuts one monomer

at a time. These motors are able to ratchet thermal fluctuations just as the ratchet and pawl mechanism proposed by Lippman but without the need for a temperature gradient. Collagenase, cellulase, chitinase, ParABS and influenza are examples of naturally occuring BBRs. Each of these have been modelled and observed.

One of the first observations of a natural BBR was that of matrix metalloproteases 1 (MMP-1) operating on collagen substrate [15]. Collagen, the most common component of extracellular matrices, is a polymer consisting of a triple helical structure that can self-assemble into fibrils of 500 nm in diameter. Collagen is resistant to degredation by non-specific proteases, however, MMP-1 is a specialized enzyme that is capable of cleaving collagen at single sites. A bound MMP-1 undegoes a biased random walk along a collagen fibril by cleaving sites spaced greater than 300 nm apart. In an experiment by Saffarian et al., MMP-1s were fluorescently tagged and their trajectories were compared with a free diffusion model [15]. The MMP-1s were found to have a transport velocity of $\sim 4\,\mu$m/s. The absence of ATP during this ballistic motion and the lysis of collagen fibrils demonstrated that motors could operate using a burnt-bridge ratchet mechanism.

Further work by the same group affirmed these findings. They showed that the motion of a cousin of this enzyme, MMP-2, was dependent on its enzymatic activity [75]. Active wild type MMP-2 trajectories were compared with mutated MMP-2 which was enzymatically inactive. The wild-type MMP-2 displayed similar behavior to the previous study by Saffarian et al. with a transport velocity of $5\,\mu$m/s, while the enzymatically inactive MMP-2 displayed purely diffusive behavior. These experiments were among the first to demonstrate in vivo BBRs as viable motors. Prior to the BBR mechanism of collagenase, linear motion was thought to be generated nearly entirely by ATP or GTP [29]. Saffarian et al. demonstrated that simply the asymmetry of interacting and non-interacting sites was sufficient to provide motion [75].

Cellulase, another enzymatic motor, demonstrated BBR behavior. Cellulase consists of two domains connected by a linker; the first is the catalytic domain that may cleave cellulose into its constituents, the second is the carbohydrate binding module that assists in peeling cellulose from the surface [76, 77]. A study by Ting et al. showed that a motor running along cellulose may be optimized by altering the interactions between the two domains, specifically the linker stiffness and length [78]. They use a mechanochemcial model in which the domains are approximated as random walkers whose relative positions affect the total energy of the system. The linker was approximated as a spring of a given length. Steady-state velocities and separation lengths were determined by minimizing the energy. The separation distance between the domains displayed interesting interplay in minimizing the energy. The carbohydrate binding module is able to lower the energy as it neared the catalytic domain by peeling cellulose from the surface, however, this comes at the cost of increasing the energy of the linker. They found that the motor runs at greatest speeds when the distance between the domains fluctuates the greatest. When separation

fluctuations are greatest, the motor transitions from a compressed state to an extended state frequently. I think the motion of this enzyme resembles the motion of an inch worm in a similar way to the DNA spider presented by Samii et al.[25]. In this way, the carbohydrate binding module may assist in releasing cellulose and then push away from the catalytic domain so that it does not obstruct motion [78].

Chitinase was also proposed to function as a BBR by Nakamura et al [68]. Chitinases are found all over nature, in bacteria, protists, fungi, plants and animals and are involved in digestion, molting, immunity and pathogenicity [79, 80]. Chitinase functions as a BBR motor by running along a chitin polymer, cutting off each monomer at each cycle and ratcheting the enzyme forward as shown in Figure 1.3 [68]. In a model by Okazaki and Nakamura, chitin was considered to be embedded in the surface on which a chitinase motor traveled [81, 82]. The chitin backbone is pulled up by the motor, requiring some free energy consumption. The motor would then oscillate between a forward and backward position and cut the polymer at a given rate. Once the polymer was cut, the motor would be forced to move forward and may peel additional chitin from the surface. Experimental observations of this motor show the motor taking one step forward, stalling for a short time followed by another step [82]. Due to the characteristic stepping followed by irreversible change in the substrate, the free energy landscape was modelled with harmonic potential wells set next to each other such that the motor could oscillate between the forward and backward states. The two wells were separated by a barrier which could be passed by sufficiently large thermal fluctuations. To emulate the cutting of chitin polymer, while in the forward potential well, the motor had some probability of completely altering the free energy landscape; the free energy landscape was altered by making a translation in the direction of motion and by lowering the energy, making backward movements energetically unfavorable. A forward-backward algorithm was used to predict the free energy landscape for a given trajectory [83]. The algorithm was run on experimental data of single chitinase motors tagged with gold nano particles, and was able to explain the particle motion with the free energy landscape model. These kinds of free energy landscape models are valuable tools in characterizing, understanding and predicting molecular motor dynamics.

In recent years, studies have demonstrated that the ParABS system uses a BBR mechanism in plasmid patterning [23, 84]. ParA decorates the nucleoid non-specifically, ParB is bound to the plasmid at ParS sites, and forms a complex that can interact with ParA. ParS is the DNA sequence that ParB recognizes on the plasmid [20]. In contrast to the originally considered polymerization partition by method in which an actin-like ParA filament connecting two identical plasmids continually grows pushing the two plasmids to either end of the cell, a BBR model is better able to explain characteristic plasmid motion [85]. Particularly, studies provide evidence contradicting a polymerization method by noting the observations of P1 ParA binding to nonspecific DNA as well as the cycling between DNA-bound and non-bound states [86]. Modelling efforts demonstrated that a BBR mechanism was able to

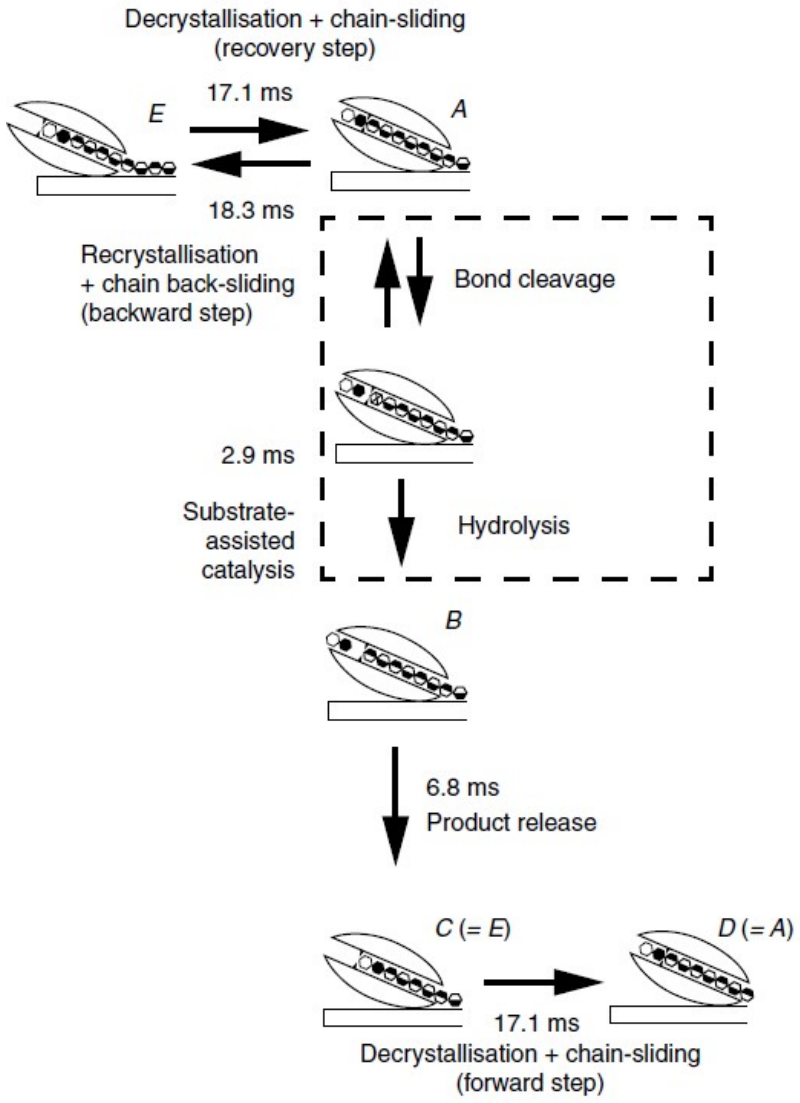

Figure 1.3: **Summary of processive chintase reaction cycle.** Chitinase may slide forward or backward by one dimer (E-A). After a single dimer is cleaved from the chain the enzyme is prevented from stepping backwards (A-B). Finally, the motor may return by dimer release and forward chain sliding (B-E). *Credit Nakamura et al. (2018)* [68]. Images reproduced with permission from the owners.

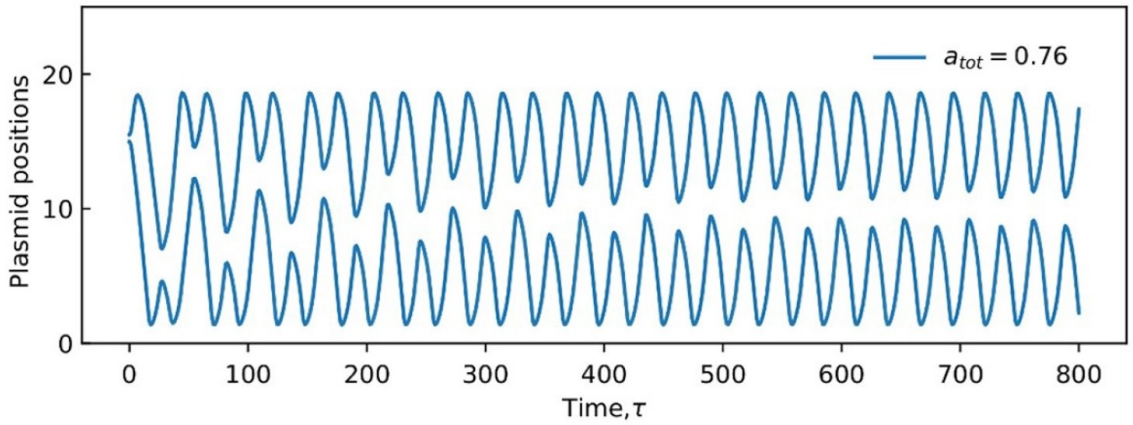

Figure 1.4: **Plasmid segregation via BBR mechanism.**The positions of two ParB complexes over time governed by the model presented by Jindal et al. Two partition complexes spontaneously segregate and then oscillate within separate regions of the surface. *Credit Jindal et al. (2019)*[23]. Images reproduced with permission from the owners.

predict and explain the motions of bacterial plasmids inside a cell [23, 87, 88, 89, 90]. Figure 1.4 shows partitioning of plasmids on a finite substrate as governed by the BBR model developed by Jindal et al. In their models ParB coated plasmids were continually guided by a nucleiod-bound ParA gradient that was consumed by ParB. Due to the elasticity of the nucleoid, binding of ParA to ParB resulted in driving force on the plasmid [87]. The gradient of ParA in front of the plasmid meant that more binding would occur in this direction and would then provide a net force to bias motion in a single direction. The 'burning' of ParA from the nucleoid would force the plasmid to be self avoiding. The plasmid's oscillatory and equal spacing behavior were each accounted for by the BBR mechanism [23, 84].

As one final example, Ziebert et al. provided a model for the rolling of a single influenza virus on the extracellular matrix [26]. Influenza contains 2 different kinds of spike proteins on its capsid membrane, namely Hemaglutinin (HA) and Neuraminadase (NA). In most influenza subtypes these two spike proteins are independent of each other and interact with substrate on their own. HA is able to bind to sialic acid residues of glycan proteins found in the extracellular matrix. NA is able to cleave sialic acid from glycan leaving a wake of non-interactive substrate where the virus has passed over (Figure 1.5). The binding and cutting process generates the chemical gradient needed for a BBR motor to function, and the influenza virus may explore regions of the matrix at a much higher rate than a purely diffusive walker. In their model, they considered a sphere rolling with a constant velocity under a given load. The sphere is able to bind and unbind at given rates and interact with substrate between two critical angles. They showed that with HA and NA working together the motor is able to traverse substrate of varied concentrations and landscapes demonstrating the motor's robustness.

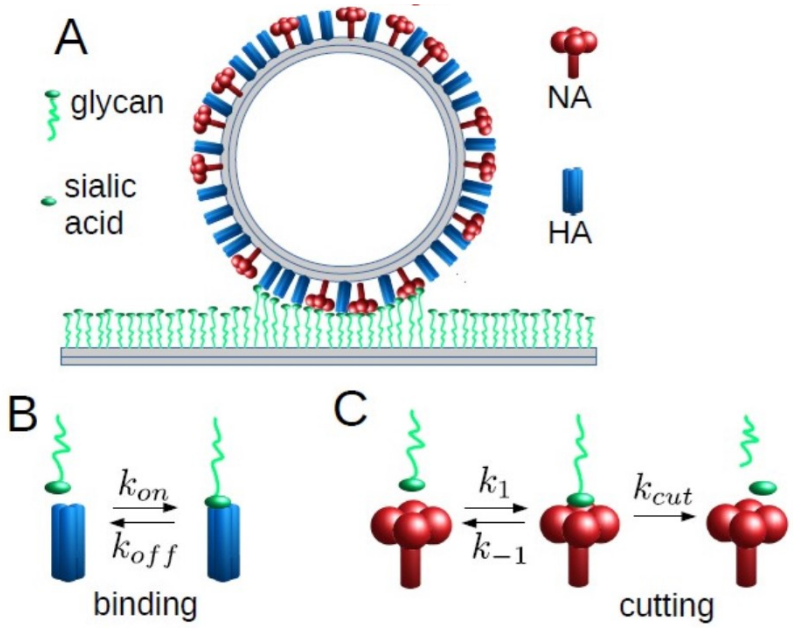

Figure 1.5: **BBR model of influenza.** (A) The influenza capsid contains two spike proteins that interact with substrate differently. (B) HA binds and unbinds substrate at given rates. (C) NA binds and unbinds substrate as well as cleaves substrate at given rate. *Credit Ziebert et al. (2021)* [26]. Images reproduced with permission from the owners.

The surge of discoveries of BBR motors throughout biology and the observation of their effectiveness, utility and resilience in unfavorable conditions provided further inspiration for the development of synthetic BBRs. BBRs were highlighted as a viable mechanism in addition to the synthetic motors already being created.

1.3 Synthetic Molecular Motors

The ubiquity of molecular motors in Nature highlights the utility they provide to every kind of living thing. This notion was not lost on chemists and biophysicists, and the search for methods, compounds and systems that can facilitate synthesis or reconstitution of molecular motors of any kind has been ongoing for decades.

Among the earliest successful syntheses was the ratchet and pawl motor by Kelly et al. [10]. They used a triptycene-helicine compound in which the two residues were connected by a single bond and able to rotate relative to one another. The ratchet was initialized with a single NH_2 branch on one of its wings that discouraged unidirectional slippage past the pawl until the wing reacted with an external agent. Once this wing slipped over the pawl it interacted with another domain of the helicene that induced a conformation change on the wing, returning it to the NH_2 state and discouraging backward motion [10].

While this motor demonstrated a proof of concept for unidirectional motion, it was a different design by Koumura et al. that showed persistent unidirectional motion [11]. In their

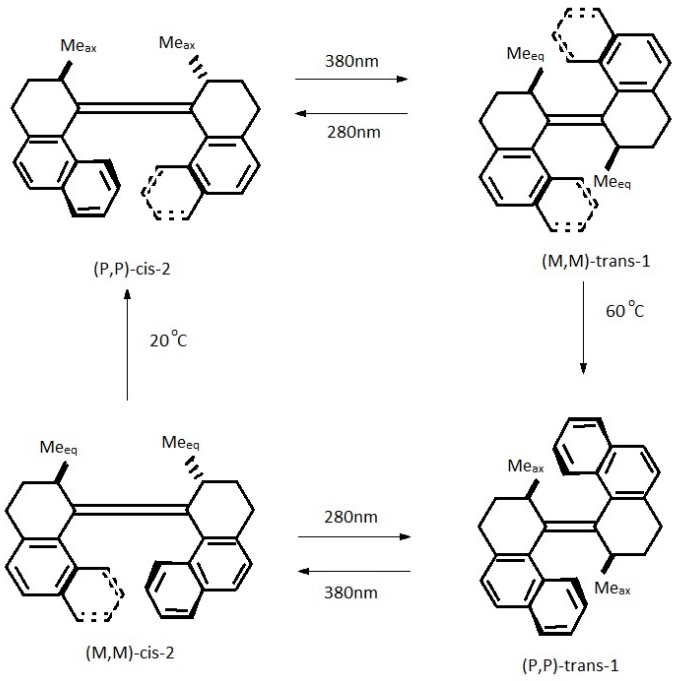

Figure 1.6: **Synthetic rotor schematic.** Photochemical and thermal isomerization cycle of rotary motor by Koumura et al. A specific stimulus is required for the motor to transition between each state [11].

design, the unidirectional conformation cycle of octohydro-dimethyl-biphenanthrylidene consisted of 4 stages: two light-induced change in chirality steps and 2 thermally induced conformation altering steps. Figure 1.6 shows the light and thermal stimulated cycle which permits rotary motion.

Constructions of light stimulated rotors, along with rotaxane and catenane based shuttles came with problems such as their lack of autonimous motion. Many of the early motors needed constant supervision and environmental changes in order to generate directed motion [34, 37]. As the bottom-up approach of designing motors by synthesizing compounds of well characterized chemistry to emulate components of conventional engines began to stall, scientists started to take inspiration from nature where autonomous, effective molecular motors were found in abundance.

While the construction of motors from their base constituents is extremely difficult, some groups were able to reconstitute known in vivo motors by utilizing large components of biologically assembled motors. Vechiarelli et al. reconstituted the F and P1 plasmid partition complexes in a cell-free system, in which a plasmid decorated with ParB traversed a DNA-coated surface bound by ParA [19]. For both F Sop and P1 Par, they found that reconstituted partition complex clusters could deplete swathes of the ATP infused, DNA coated surface.

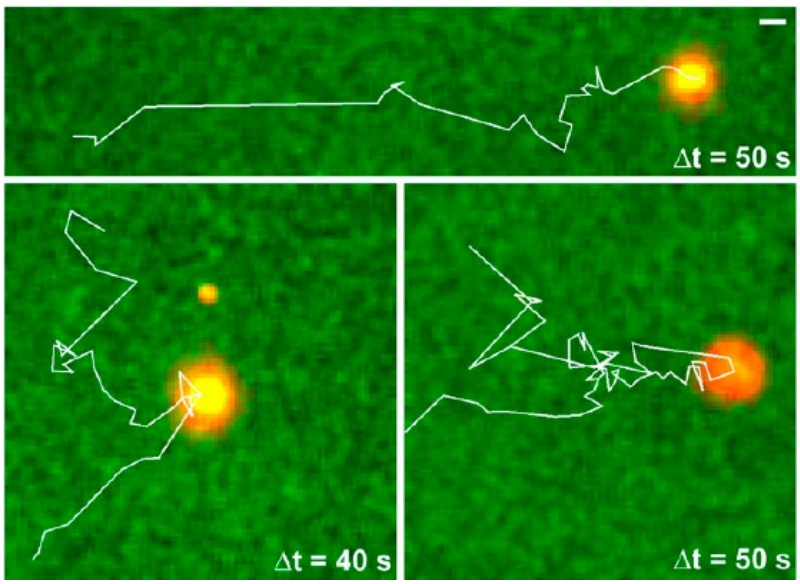

Figure 1.7: **Sample trajectories of P1 plasmids over a DNA susbtrate.** The bright spot indicates the initial position of the plasmid, and white lines indicate the path of the partition complex. P1 plasmid cluster split into smaller complexes leading to two separate paths. *Credit Vecchiarelli et al. (2013)* [19]. Images reproduced with permission from the owners.

The DNA in the carpet remained mostly intact while the ATP was hydrolysed indicating that the source of energy for the motor was stored in ATP bound to the surface [19]. Figure 1.7 shows sample trajectories of reconstituted P1 plasmids moving across a DNA-saturated carpet.

Molecular motors based entirely on DNA have also been synthesized and bring with them many benefits. DNA-based motors were more easily tuned to the needs of the experimentalist due to their well understood and closely followed assembly rules. As well, DNA as a whole has been extensively researched providing numerous methods with which to design and create any nucleotide sequence [91].

DNA walkers resembling the motion of kinesin and dynein used multiple legs to progress down a track. These so called DNA spiders attach to complementary DNA preset along a track. The first leg attaches to a site followed by a detachment and reattachment of the other leg farther along the track. Each detachment is accompanied by a cleavage and dissociation of the track-bound DNA at that site, thus the motor is forced to continue along the track and avoid moving where it had previously stepped. Sherman and Seeman developed a DNA spider that moves along a linear track in an inchworm fashion with the back leg following the lead leg [92, 93]. Figure 1.8 shows the schematic of another spider developed by Shin et al. that was able to have each leg step one over the other as with kinesin and dynein. The design by Shin et al. involved specific DNA that would facilitate each leg binding and unbinding to the track [94]. With this mechanism each attachment and detachment DNA strand would be site specific, so the set of strands would need to be added

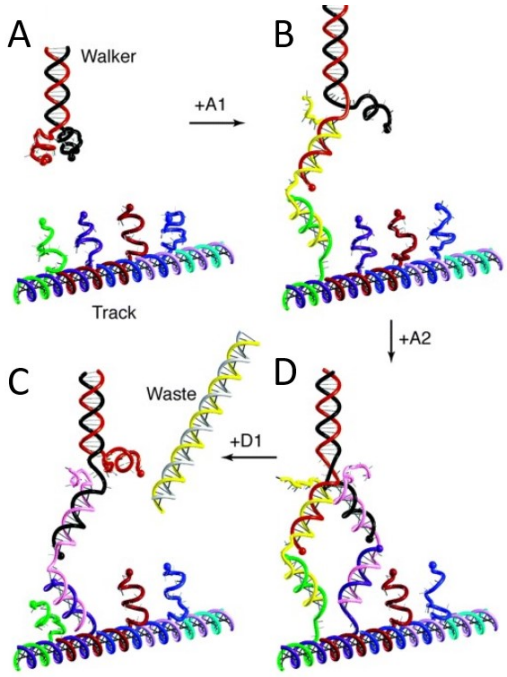

Figure 1.8: **Schematic of DNA walker locomotion.** Colored spheres on the end of each leg and binding strand represent dyes (HEX, green; Cy5, purple; FAM, red; Texas Red, blue) and quenchers (BHQ1, orange; IBRQ, black) for detecting walker movement. The diagrams depict (a) unbound walker, (b) walker attached to branch 1, (d) walker attached to branches 1 and 2, and (c) walker released from branch 1 to yield duplex waste. Reprinted with permission from [94]. Copyright 2004 American Chemical Society). *Credit Shin et al. (2004)* [94]. Images reproduced with permission from the owners.

to the system sequentially. The obvious limitation with this motor being its non-autonomy and the extensive work needed to construct the track and site specific attachment and detachment strands.

Work by Pei et al. demonstrated a DNA spider that was able to autonomously move over a substrate-decorated surface [38]. They constructed polycatalytic assemblies, capable of continuously diffusing across a surface through biased diffusion. They demonstrated that the motility of the spider and rate of substrate consumption could be adjusted by changing the amount of surface binding sites and the number of legs on the spider. In their setup, varying amounts of deoxyribozymes, DNA oligonucleotides, were coupled with streptavidin, the deoxyribozymes could then bind to complementary DNA at each binding site. The deoxyribozymes functioned as the legs that could processively attach and detach to substrate and the streptavidin functioned as the body of the spider. Once attached to substrate, each leg could cleave the substrate at some rate, after which each leg's affinity for the substrate would be decreased (although not eliminated). They were able to change the strength of leg-substrate binding by simultaneously adjusting the length of the interaction regions in the legs and substrate; a longer interaction region led to greater

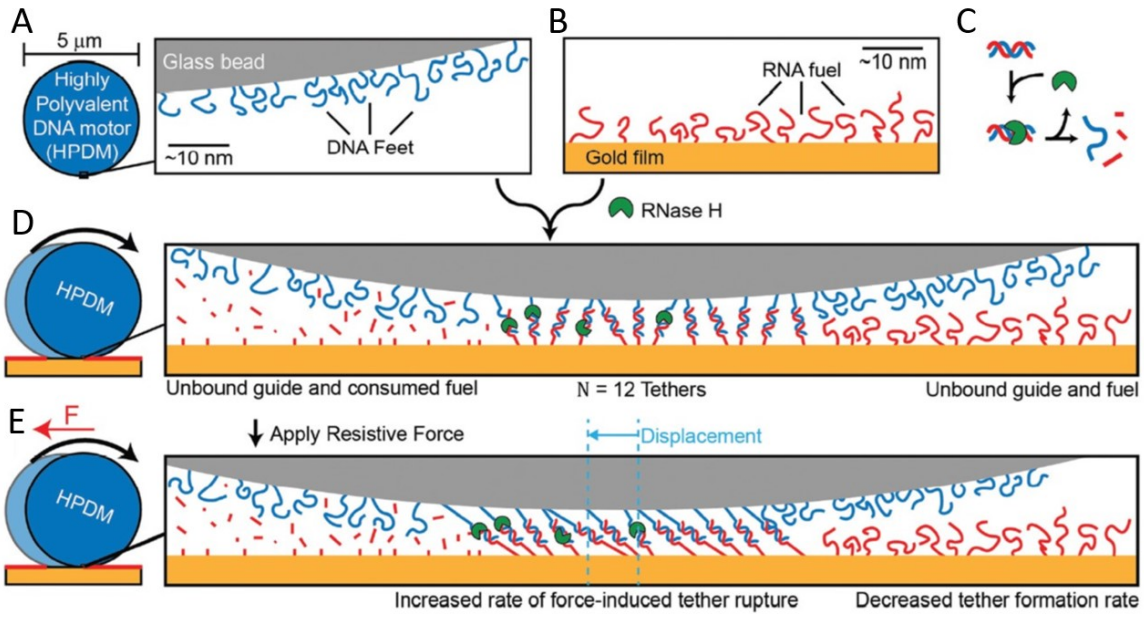

Figure 1.9: **Depiction of the polyvalent DNA motor.** (a) The motor hub (grey) is coated with single stranded DNA (blue). (b) These DNA bind RNA (red) strands that are attached to a gold surface(yellow) to form "tethers". (c) Tethers are cleaved by the enzyme RNase H (green), which selectively degrades the RNA in DNA–RNA duplexes. (d) RNase H promotes processive motion by continuously cleaving tethers, causing the motor hub to move and bind new tethers, leaving a fuel "depletion zone" in its wake. (e) The motor is able to overcome resistive forces and maintian forward motion. *Credit Blanchard et al. (2021)* [24]. Images reproduced with permission from the owners.

binding strength. They demonstrated that processivity could be increased by increasing the strength of binding between the legs and substrate as well as increasing the number of legs.

Later, a protein based, polyvalent, rolling motor was created by Korosec et al. [74]. The motor consisted of a spherical hub decorated with trypsin proteases and a peptide substrate bound to a surface. The motor was able to undergo super-diffusive motion through trypsin-substrate binding followed by the cleavage of substrate from the surface. This was the first synthetic molecular motor to use neither natural motor-protein components nor DNA.

Finally I address the findings of a DNA-RNAse motor by Blanchard et al. [24, 43]. In their design, shown in Figure 1.9, a monowheel decorated in single-stranded DNA interacts with an RNA covered surface. The single stranded DNA contains portions of a sequence that is complementary to the RNA fuel; in this way the DNA and RNA may form several hydrogen bonds allowing the hub to interact with the substrate. The RNA-DNA binding allows the motor to pull itself along the surface through elastic restoring forces, while RNase continually cuts the bonds at a given rate. In this way the motor functions as a BBR and is able to generate consistent directed motion.

The group was able to demonstrate the stall force and motility may be adjusted by altering the substrate density, polyvalency and the DNA leg "span". The "span" quantifies

the number of RNA fuel available to a given DNA strand. They showed that increasing polyvalency increased the processivity and motility of the motor. The motor displayed bursts of speed of near 50 nm/s. Trajectory mean squared displacements (MSD) were fitted with power laws and showed that the particles exhibited superdiffusive exponent values (~ 1.5) and this exponent could be maximized by altering the polyvalency and DNA leg span. As well, the processivity increased with the DNA leg span as this resulted in the largest portion of DNA strands binding to the surface [22]. They also demonstrated that such motors moved by a rolling mechanism. In one experimental setup, Blanchard et al. attached stretavadin bound with biotin and single stranded DNA to the motor-bound DNA by DNA-DNA base pairing [43]. The stretavadin-biotin complex would securely attach to the surface and would be impervious to the RNase H such that the only means of the motor breaking the bond would be to rupture the DNA-DNA hydrogen bonds. This rupture force was known to be around 49 pN, so the streptavidin-biotin complex could be used as a force measuring tool if its concentration was known. Remarkably they found that the motor hub was able to overcome forces of around 150 pN, far exceeding the stall force of previously known motors.

These remarkable discoveries demonstrate the viability of BBRs as the future of synthetic molecular motors. The ability to complete nano-scale tasks within a wide range of environments opens up numerous possibilities limited perhaps only by our own creativity. However, much remains to be understood and better characterised before the full utility of BBRs as molecular workers may be realized.

1.4 Thesis organisation

This thesis is organized as follows: in Chapter 2, I provide a deterministic model for a polyvalent motor hub utilizing a BBR mechanism, which complements prior modelling work [23]. I consider a motor hub interacting with a surface decorated with substrate, in which the substrate may exist in one of three states. The dynamics of the hub are sensitive to several system parameters which are tuned to reveal parameter dependencies. I find that total substrate concentration as well as state transition rates influence motor motility and efficiency. I map the parameter space to determine optimal efficiency and motility and find interesting insights that experimentalists may use to optimize in vitro motors. This work has been published [95].

In Chapter 3, I extend the model to include diffusion of the motor hub. I consider the motor hub to be interacting with the same surface in which the hub undergoes one-dimensional Brownian motion in addition to the forces of the interactions with the substrate. I observe the effects of the substrate concentration, substrate burn rate and diffusion coefficient on the motility and efficiency of the motor. I also look at the time dependence of the velocity and characteristic motion.

In Chapter 4, I summarize my thesis by reviewing the main findings from Chapters 2 and 3. In addition, I outline future investigations and extensions to the models discussed in this thesis that may help understand the mechanism underlying other biological or synthetic systems based on the burnt-bridge ratchet mechanism.

Chapter 2

Optimizing efficiency and motility of a polyvalent molecular motor

2.1 Introduction

Previous experimental and theoretical work has helped to uncover the physical and chemical mechanisms that drive the motion of BBRs. Several reconstitution efforts have demonstrated the viability of synthetic BBRs. Vechiarelli et al. reconstituted the SopABC system and demonstrated that the motility could be adjusted by altering system parameters such as chemical kinetics and substrate concentration [19]. Using DNA–RNA binding, another cell-free study by Blanchard et al. demonstrated that motors could move against large persistent forces and interact with thousands of substrate molecules simultaneously [24, 43]. Substantial work has also been conducted to produce in vitro BBRs in which the bond strength for each substrate-motor bond could be altered by adjusting the motor-substrate binding energy [19, 38, 43]. By adjusting the bond strength it is possible to tune the rate of force-dependent unbinding. Additionally, ParAB inspired models have shown that the substrate concentration is proportional to the motor's steady-state speed and the speed could be optimized by altering substrate to motor interaction lengths [88].

The above work has focused on the motility of BBRs and their optimization—their speed, persistence and processivity. However, these systems are driven far from equilibrium and have a constant source of chemical energy that powers their motion, and so, how can one optimize their efficiency? In motors such as kinesin and F1-Atpase that have an active power stroke, the efficiency is well characterized, reaching as high as 40–80% and nearly 100% respectively [59, 96, 97]. With respect to BBRs, they rectify thermal motion without any power stroke, and so, by definition, will be less efficient due to the system being far from equilibrium. Nevertheless, it has not yet been established how a BBR's efficiency depends on its chemistry and force generation. For instance, will a BBR be more efficient at low or high burn rates, and is it better to have a high or low concentration of substrate?

In this chapter, I explore how to optimize the efficiency of a polyvalent motor hub undergoing burnt-bridge ratcheting using a deterministic model. The motor binds substrate and catalyzes its removal at some burn rate. From the motion of the motor and its rate of substrate consumption I calculate its Stokes efficiency, which is the ratio of the output power (against the drag force) to the rate of chemical energy input [54]. I find that for a fixed amount of substrate, the optimal efficiency occurs at an intermediate substrate consumption rate. I also consider force-dependent unbinding of the motor from the substrate, and find that under certain conditions it is favourable to have some unbinding for more efficient operation. Thus, it is possible that a motor which burns every single substrate it comes in contact with can operate less efficiently than one which can unbind substrate. Our findings lead to testable predictions, in particular, for in vitro synthetic burnt-bridge ratchets where both the binding and unbinding kinetics can be tuned.

2.2 Materials and Methods

In our model, a polyvalent motor hub interacts with substrate molecules that are attached to a surface of polymers (see Figure 2.1), or are themselves polymers such as in the DNA-RNAse-based systems. I assume that the hub's motion is confined to one dimension. The substrate can exist in one of three states: (i) surface-bound, (ii) bound to the hub and the surface or (iii) free in the buffer (Figure 2.1A). (This extends our previous model that did not explicitly consider the dynamics of the bound complex [23, 88].) The concentration of surface-bound substrate on the track at position X is $A_s(X)$. The hub can bind to surface-bound substrate and form a complex leading to a concentration of bound complex at X given by $A_c(X)$ (Figure 2.1B). Substrate in the complex can be dissociated and released back into the buffer where it is in the free state and has a concentration A_f that is independent of position since I assume that the buffer is well mixed. Substrate in the buffer can bind to the surface at a rate constant, k_{on}, and can also unbind at a rate constant k_{off} (Figure 2.1C). The system is closed and starts with an initial substrate concentration, A_{tot}. At all future times the substrate concentration satisfies $\int A_{\text{tot}} dX = \int A_f(t) dX + \int A_s(X,t) dX + \int A_c(X,t) dX$.

When the hub is bound to a substrate, the complex experiences a linear restoring force due to the entropic elasticity of the underlying surface to which the substrate is attached. The total force from the bound complex on the hub, located at X_h, is then

$$F = \int -k(X_h - X) A_c(X) dX \,,$$

where the entropic elasticity is given by the effective spring constant, $k = \frac{k_B T}{\sigma^2}$, σ is the characteristic fluctuation length of the polymers and $k_B T$ is thermal energy. The dynamics of the hub are in the over-damped regime and so the elastic force is balanced by the drag

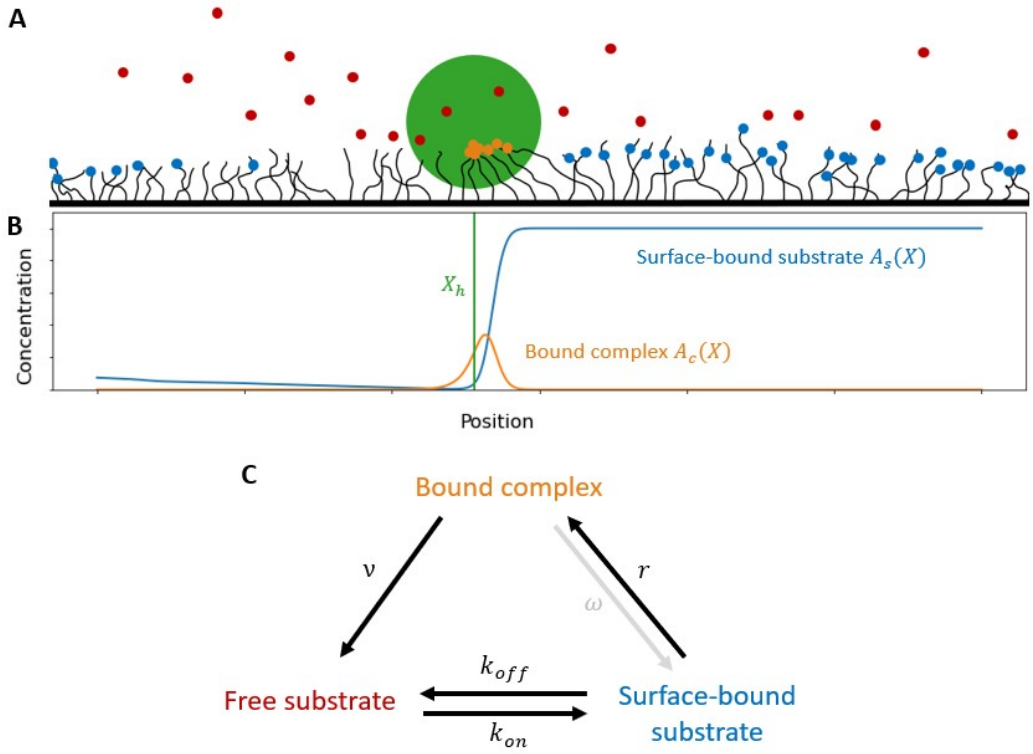

Figure 2.1: **Model schematic.** (A) The motor hub (green) interacts with surface-bound substrate (blue) forming bound complex (orange) which is eventually burnt and freed to the buffer (red). (B) Example concentration of surface-bound substrate and bound complex and the relative location of the hub at a single point in time. (C) Schematic of state transitions and associated rates. The bound complex to surface-bound state transition is initially ignored.

force. The equation of motion for the hub is

$$\gamma \frac{dX_h}{dt} = -\int k(X_h - X) A_c(X)\, dX\,, \tag{2.1}$$

where γ is the viscous drag coefficient. For a spherical particle moving through bulk, this may be approximated as $\gamma = 6\pi\eta' R$, where η' is the fluid viscosity and R is the radius of the particle. However, due to hydrodynamic effects near boundaries, this expression breaks down [98]. Nevertheless, I assume the hub is constantly tethered to the surface during its motion and is therefore at a constant height. So the drag coefficient is constant, albeit larger than what it would be in bulk solution.

As the surface polymers fluctuate, the surface-bound substrate moves either further or closer to the hub. Those that come in contact with the hub form a bound complex at rate r. The energy of the fluctuation is $\frac{1}{2}k(X - X_h)^2$; assuming that these fluctuations are in equilibrium compared to the timescale of the motion of the hub, the rate of complex formation obeys Arrhenius kinetics with $r \exp\left[-\frac{\beta}{2}k(X - X_h)^2\right] A_s(X)$. $\beta = \frac{1}{k_B T}$ is the inverse thermal energy. The hub then catalyzes the dissociation of substrate in the bound complex to the free state at a burn rate constant ν. For now, I will assume that there is no unbinding of bound complex back into the surface-bound state; this will be added later. The chemical kinetics for the bound complex using the above assumption is

$$\frac{dA_c(X)}{dt} = re^{-\frac{\beta}{2}k(X - X_h)^2} A_s(X) - \nu A_c(X)\,. \tag{2.2}$$

The dynamics of surface-bound substrate has several contributions, including the loss due to the formation of the bound complex. I assume that it can unbind and return to the buffer at a rate constant k_{off} and free substrate in the buffer can bind to the surface at a rate constant k_{on}. I assume that the motor is small compared to the surface. In other words, I assume we are in the limit where the amount of bound complex compared to the total substrate concentration is negligible (i.e. $A_{\text{tot}} \approx A_s + A_f$). I also assume that the buffer has come to steady-state with the surface so that . Under these assumptions the binding rate, $k_{\text{on}} A_f$ at steady-state is

$$k_{\text{on}} A_f = \frac{k_{\text{off}}}{(1 + k_{\text{off}}/k_{\text{on}})} A_{\text{tot}}$$

(See Appendix 2.5.2 for full derivation.)

The full chemical kinetics of the surface-bound substrate then follows

$$\frac{dA_s(X)}{dt} = \frac{k_{\text{off}}}{(1 + k_{\text{off}}/k_{\text{on}})} A_{\text{tot}} - k_{\text{off}} A_s(X) - re^{-\frac{\beta}{2}k(X - X_h)^2} A_s(X)\,. \tag{2.3}$$

Equations (2.1)–(2.3) can be non-dimensionalised using the substitutions $X = \sigma x$, $t = \frac{\tau}{r}$ and $A_i(x) = a_0 a_i(x)$, leading to the following dimensionless equations,

$$\frac{dx_h}{d\tau} = -\int (x_h - x) a_c(x)\, dx\,, \tag{2.4}$$

$$\frac{da_c(x)}{d\tau} = e^{-\frac{(x-x_h)^2}{2}} a_s(x) - \nu' a_c(x)\,,$$

$$\frac{da_s(x)}{d\tau} = \frac{k'_{\text{off}}}{(1+K)} a_{\text{tot}} - k'_{\text{off}} a_s(x) - e^{-\frac{(x-x_h)^2}{2}} a_s(x)\,,$$

where $\nu' = \frac{\nu}{r}$, $K = \frac{k_{\text{off}}}{k_{\text{on}}}$ and $k'_{\text{off}} = \frac{k_{\text{off}}}{r}$. I define the reference concentration to be $a_0 = \gamma r \sigma / k_B T$. (Note that this reference concentration depends on the size of the hub through γ, its ability to bind substrate through r, and the characteristic fluctuations of the underlying surface σ. Changing any of these is effectively equivalent to changing the substrate concentration.) Thus, the dynamics of the hub depends on four dimensionless parameters: the total substrate concentration, a_{tot}, the hub induced substrate burn rate constant , ν', the substrate equilibrium constant, K, and the free unbinding rate of surface-bound substrate k_{off}. Table 2.1 provides an overview of the characteristic quantities used for non-dimensionalisation. I assume that the chemical kinetics governing substrate binding to the surface is similar to its binding with the hub and so for simplicity, I set $k_{\text{on}} = r$. Thus, $K = k'_{\text{off}}$ in our simulations.

Table 2.1: Characteristic quantities

Quantity	**Characteristic quantity**	**Symbol**	**Typical value**	**Non-dimensionalised quantity**
inverse time	complex formation rate constant	r	$20s^{-1}$ [24]	$\tau = rt$
length	characteristic fluctuation	$\sigma = \sqrt{k_B T / k}$	$100nm^{\dagger}$	$x = X/\sigma$
concentration	reference concentration	$a_0 = \gamma r \sigma / k_B T$	$10\mu m^{-1\ddagger}$	$a_{\text{tot}} = A_{\text{tot}}/a_0$

† Calculated using using $k_B T = 4.1 pN nm$ and $k \sim 0.2 pN/\mu m$ [99]. ‡ Calculated using $\gamma = 6\pi\eta' R$, where $\eta' = 10^{-3} Pa\,s$ [44] and $R \sim 1\mu m$ [43]. For reasons mentioned earlier, this value for the drag coefficient should be viewed as a lower bound.

2.2.1 Force-Dependent Unbinding

In the above, I made the assumption that all substrate bound to the hub could never unbind and would eventually get burnt. Here, I relax that assumption and allow the complex to dissociate back to its surface-bound state at a rate constant ω. I also allow for this to have an additional force dependence due to the restoring force pulling on the substrate-hub bond. This is parameterized by δ, the distance to the transition state. The energy difference between the bound complex and surface-bound state due to the work performed by the restoring force is

$$\delta E = -F(X)\delta = -k|X_h - X|\delta\,.$$

The kinetics for the bound complex and surface-bound substrate become

$$\frac{dA_c(X)}{dt} = re^{-\frac{\beta k}{2}(X_h - X)^2}A_s(X) - \nu A_c(X) - \omega e^{\beta k|X_h - X|\delta}A_c(X)\,,$$

$$\frac{dA_s(X)}{dt} = \frac{k_{\text{off}}}{(1 + k_{\text{off}}/k_{\text{on}})}A_{\text{tot}} - k_{\text{off}}A_s(X) - re^{-\frac{\beta k}{2}(X_h - X)^2}A_s(X) + \omega e^{\beta k|X_h - X|\delta}A_c(X)\,.$$

These can be non-dimensionalised by following the same substitutions as above in addition to setting $\delta = \frac{\delta'}{\sigma}$ and $\omega = \omega' r$ to yield

$$\frac{da_c(x)}{d\tau} = e^{-\frac{1}{2}(x_h - x)^2}a_s(x) - \nu' a_c(x) - \omega' e^{|x_h - x|\delta'}a_c(x)\,, \tag{2.5}$$

$$\frac{da_s(x)}{d\tau} = \frac{k'_{\text{off}}}{(1 + K)}a_{\text{tot}} - k'_{\text{off}}a_s(x) - e^{-\frac{1}{2}(x_h - x)^2}a_s(x) + \omega' e^{|x_h - x|\delta'}a_c(x)\,. \tag{2.6}$$

I solve Equations (2.4)–(2.6) using a 4th order Runge–Kutta method with adaptive stepping. The ODE solver package `solve_ivp` from `scipy.integrate` was used to find both the trajectory of the motor and the time evolution of the substrate concentration. The spatial coordinate was discretized with spacing of $\Delta X = 0.1\sigma$.

Table 2.2 provides an overview of system variables and typical values.

Table 2.2: Model variables

Variable	Definition	Typical value	Non-dimensionalised quantity
β	inverse thermal energy	$0.25 pN^{-1}\, nm^{-1}$	-
ν	motor catalyzed substrate burn rate constant	$\sim 20 s^{-1}$ [24]	$\nu' = \frac{\nu}{r}$
A_{tot}	total substrate concentration	$\sim 100 \mu m^{-1}$ [43]	$a_{\text{tot}} = \frac{A_{\text{tot}}}{a_0}$
k_{off}	substrate unbinding rate constant	-	$k'_{\text{off}} = \frac{k_{\text{off}}}{r}$
k_{on}	substrate binding rate constant	set to $\sim 20 s^{-1}$	$k'_{\text{on}} = \frac{k_{\text{on}}}{r}$
K	substrate equilibrium constant	-	-
ω	bound complex dissociation rate constant	-	$\omega' = \frac{\omega}{r}$
δ	distance between bound complex and transition state	-	$\delta' = \frac{\delta'}{\sigma}$
ΔG	energy released per substrate molecule	$\sim 15 k_B T$ [43]	$\Delta g = \frac{\Delta G}{k_B T}$

2.2.2 Efficiency

The efficiency of a motor is defined to be the ratio of output work (or power) to input work (or power). Many motors operate between two baths at different temperatures, where the optimal efficiency is given by the Carnot efficiency. Biomolecular motors operate in a bath that is at a fixed temperature. In the low Reynolds number regime, the efficiency is the ratio of power conducted on viscous drag force over the rate of chemical energy usage [54]. This ratio is known as the Stokes efficiency and defined as

$$\eta = \frac{\gamma V^2}{B}, \tag{2.7}$$

where V is the velocity of the hub and B is the rate of change in chemical free energy [100]. For our model I calculate $B = \Delta G \nu \int A_c(X) dX$ where ΔG is the free energy change per substrate molecule burned. Since the bound complex dissociation step is irreversible, ΔG is not well defined. However, we can make an order of magnitude approximation of the ΔG by considering how close the system is to equilibrium. The systems I consider are far from chemical equilibrium where the amount of product is small compared to consumable substrate. Thus, ΔG is many $k_B T$ and drives the conversion of substrate into product, which when coupled mechanically to the hub, can be used to do mechanical work. I wish to non-dimensionalise equation (2.7). Setting $\Delta G = \Delta g k_B T$ and making the same space, time and concentration substitutions as before, I get the non-dimensionalised numerator of equation (2.7),

$$\gamma V^2 = \gamma \sigma^2 r^2 v^2.$$

Here, $v = V/\sigma r$ is the non-dimensionalised velocity. Similarly for the denominator,

$$B = \Delta G \nu \int A_c(X) dX = \Delta g k_B T a_0 \sigma r \nu' \int a_c(x) dx.$$

Substituting each of these into equation (2.7) and recognizing that $\gamma \sigma^2 r^2 / k_B T a_0 \sigma r = 1$, I arrive at a form of the Stokes efficiency in terms of non-dimensionalised quantities,

$$\eta = \frac{1}{\Delta g} \frac{v^2}{\nu' \int a_c(x) dx} = \frac{1}{\Delta g} \frac{v^2}{b}. \tag{2.8}$$

Here, $b = \nu' \int a_c(x) dx$ is the non-dimensionalised substrate consumption rate.

2.3 Results

Here, I present the results of our deterministic model for a polyvalent hub on a substrate with total substrate concentration a_{tot} and with the hub burning the substrate at a rate constant ν' (see Figure 2.1 for schematic).

Figure 2.2A shows representative snapshots of a hub as it moves across a substrate and how the formation of bound complex establishes a surface-bound substrate gradient. In order to break symmetry and initiate motion, I set the initial concentration of the surface-bound substrate to be $\frac{a_{\text{tot}}}{1+K}$ in front with a triangular well behind. There is an initial transient period where bound complex builds up and the hub's speed changes, but at later times the hub reaches a steady-state speed and a traveling wave-front is formed in the surface-bound substrate. The non-monotonic increase in velocity during the transient is due to the initial conditions in the substrate concentration which are far from the final steady state profile, and so are not pertinent. Figure 2.2B shows the time dependence of the velocity of the hub at different burn rates, ν', for a fixed total substrate concentration, $a_{\text{tot}} = 1.0$. The initial spike in velocity results from a surplus of surface-bound substrate available to the hub. At some burn rate constant s, after the initial transient spike in speed, the hub eventually reaches a constant steady-state speed. At very high and very low burn rates the hub cannot set up a sustainable chemical gradient and its speed gradually decays. In Figure 2.2C, I show that the consumption rate, b, also peaks and reaches steady-state at similar time scales to the velocity. Notably, an increase in ν' does not necessitate an increase in b; this is due to the fact that consumption rate scales with velocity. The more surface-bound substrate the hub moves through the more substrate it consumes.

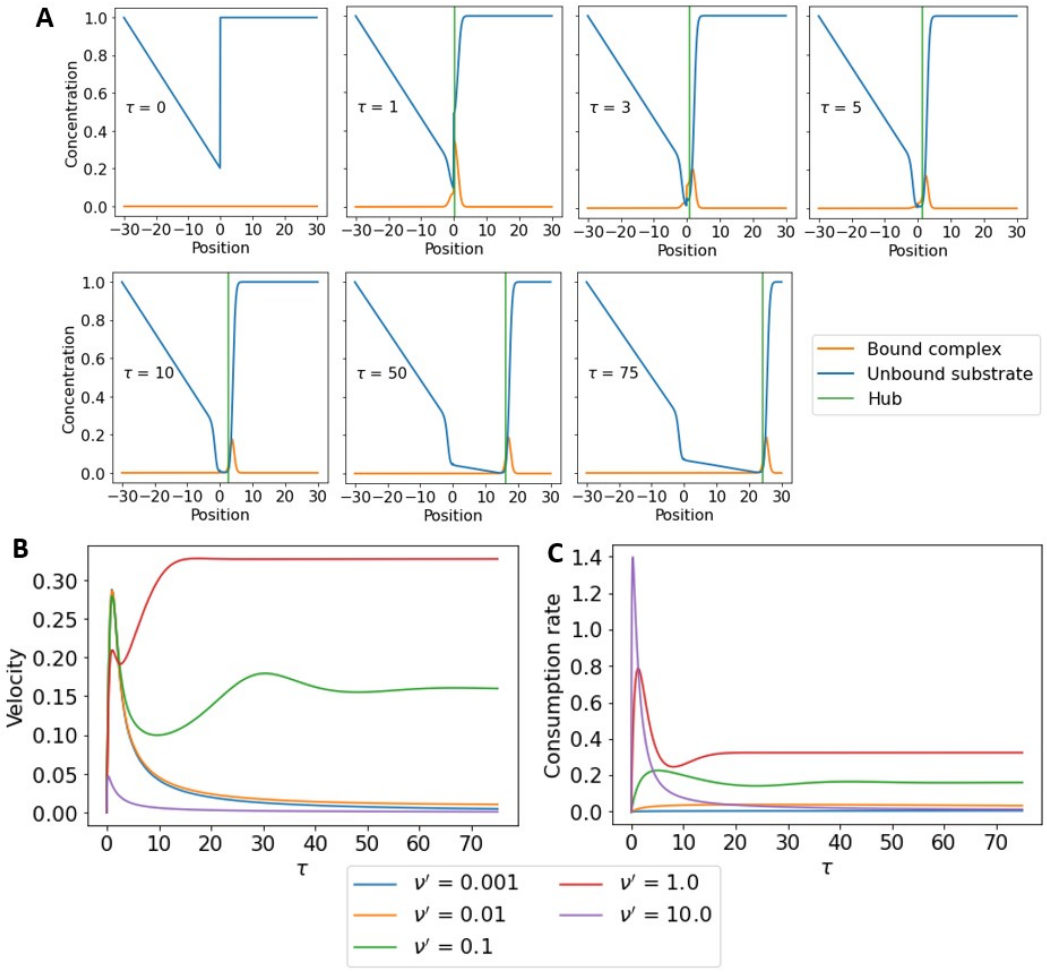

Figure 2.2: **Time dependence of hub velocity and substrate consumption rate.** (A) Substrate concentration profiles and the hub position at different points in time. (B) The velocity of the motor as a function of time at different burn rates, ν'. There is an initial transient period where the hub accelerates and attains peak speed. For some burn rates, the hub eventually achieves a constant steady-state velocity, whereas at very high or very low burn rate constants, there is a continual slowing down of the hub with time. (C) The consumption rate, b, as a function of time at different burn rate constants. The substrate consumption rate peaks and reaches steady-state at similar times to the velocity. In all of the above calculations, $a_{\text{tot}} = 1$, $\omega' = 0$, $k'_{\text{off}} = K = 0.01$.

In Figure 2.3, I show the resulting steady-state velocity and consumption rate as a function of ν' and a_{tot}. For a fixed a_{tot}, an optimal value of ν' exists that maximizes the velocity (Figure 2.3A). A ν' that is small will allow for the hub to attach to the substrate but the lack of burning does not allow for a significant gradient to form, while a large ν' quickly burns off any bonds with the substrate and again no sustained gradient is formed to drive motion. For both large and small ν', the lack of a significant chemical gradient leads to low velocity but a complete stall results from the rebinding of substrate to the surface that fills in the wake behind the hub, removing any gradient that had existed (Figure 2.3A

inset i,iii). If the burn rate constant facilitates a substantial gradient, the hub may outpace the substrate rebinding and maintain its chemical gradient (Figure 2.3A inset ii). In this case, the majority of bound complex exists in front of the hub providing a constant forward force. For fixed, v', increasing a_{tot} leads to an increase in velocity (Figure 2.3B) since additional available substrate increases the force applied to the hub. The velocity saturates due to an ever increasing 'remainder' (Figure 2.3B inset). I define the 'remainder' as leftover surface-bound substrate at the rear of the hub. The remainder is calculated by finding the minimum concentration of surface-bound substrate. Due to substrate rebinding the concentration of substrate left behind the hub continually increases until it reaches the steady-state concentration $\frac{k'_{\text{off}}}{1+K} a_{\text{tot}}$. This means that the actual remainder is found immediately after the hub had passed by. A large remainder allows for binding of substrate behind the hub, resulting in an increased backward force.

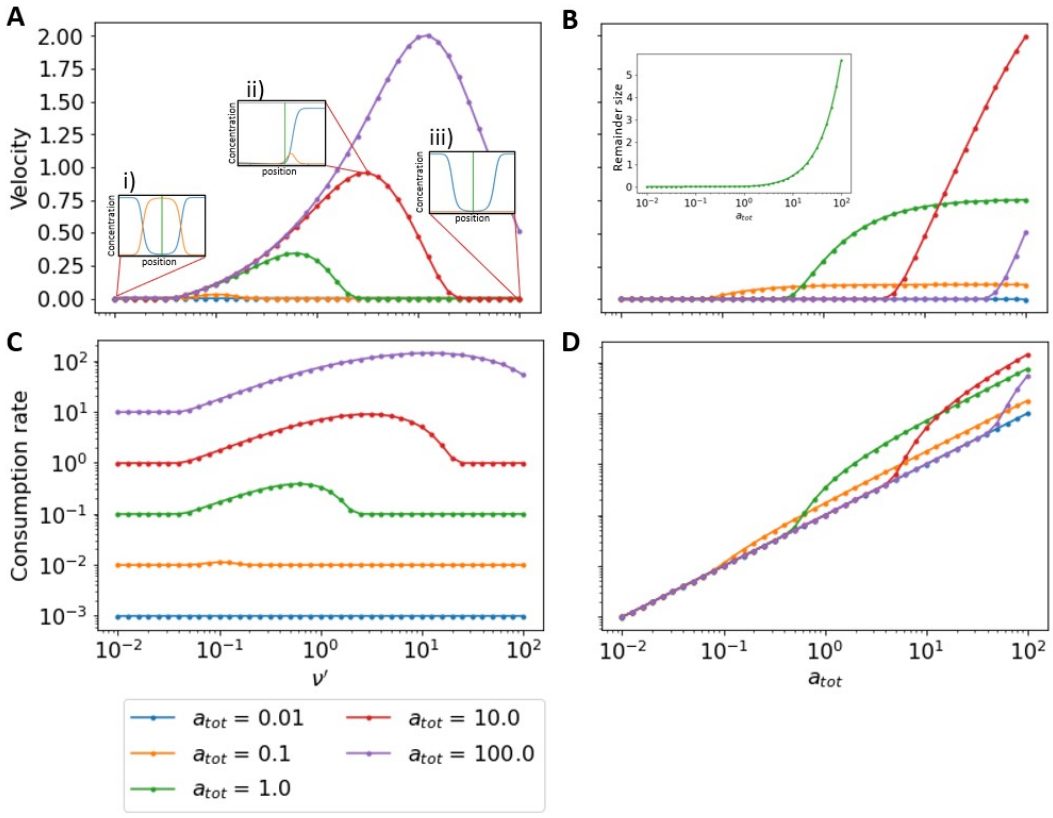

Figure 2.3: **Dependence of steady-state velocity and consumption rate on system parameters.** (A) Steady-state velocity as a function of ν' at different values of a_{tot}. At fixed a_{tot} there is an optimal, intermediate ν' that leads to the largest hub speed. (B) Steady-state velocity as a function of a_{tot} at different ν'. At fixed ν', the steady-state velocity increases with a_{tot}, but eventually saturates. (C) Steady-state substrate consumption rate as a function of ν' at fixed a_{tot}. As with velocity, the consumption rate peaks at a given burn rate constant . (**D**) Steady-state consumption rate as a function of a_{tot} for fixed ν'. At a fixed burn rate constant , the consumption rate increases without bound with increasing a_{tot}. In all of the above calculations, $\omega' = 0$, $k'_{\text{off}} = K = 0.01$.

In Figure 2.3C, I show the consumption rate of the motor as a function of the burn rate. For a given a_{tot}, the consumption rate is maximal when the velocity is greatest (Figure 2.3C). This can be understood as the hub moving through more surface-bound substrate allowing it to consume more of it. Figure 2.9 from Appendix 2.5.3 shows the velocity as a function of consumption rate; I show that the curves are closely approximated by linear equations, emphasising that $b \sim v$. Regardless of the velocity of the motor, the consumption rate is always greater than zero because of the continual rebinding of surface-bound substrate. When the velocity of the hub is zero the consumption rate is independent of burn rate constant ; this is especially clear in Figure 2.3D where consumption rate is plotted as a function of substrate concentration, a_{tot}. On a log-log plot, when $v = 0$, the slope of the curve is 1 showing that consumption depends linearly with a_{tot}. When the hub velocity

is non-zero, the consumption rate changes, but eventually, when the hub speed saturates consumption returns to scale linearly with a_{tot}. I also show that the consumption rate scales with a_{tot} by considering the steady-state surface-bound substrate concentration, a_s^*. At steady-state, $a_s^* = \frac{1}{1+K} a_{\text{tot}}$ (see Appendix 2.5.2 for derivation) indicating that a_s^* only depends on the total substrate concentration and the substrate equilibrium constant, both of which are constants. Setting Equation (2.5) to zero, at steady-state $e^{\frac{(x-x_h)^2}{2}} a_s^* = \nu' a_c^*$, therefore, a_c^* is also proportional to the total substrate concentration, therefore, $b \sim a_{\text{tot}}$.

I make use of this scaling to solve the ODEs analytically for the steady-state (see Appendix 2.5.1) and find an expression for the velocity. Under the assumption that no substrate rebinding takes place and no force-dependent unbinding occurs, the consumption rate may also be approximated by assuming the hub consumes all the substrate that it passes over (see Figure 2.8) and this allows for approximations of the steady-state efficiencies (see Appendix 2.5.1). Figure 2.7 compares the analytic approximations with the simulated results. I find that the two results are in agreement for velocities above a stalling value and where the previous assumption (that the hub consumes all substrate it passes over) holds.

Using our results for the hub's velocity, v, and the substrate consumption rate, b, I calculate the Stokes efficiency of our hub as a function of the chemistry. For fixed a_{tot}, there is an optimal efficiency at a specific ν' (see Figure 2.4A). Slow and fast burn rate constants lead to a stalled motor and hence zero efficiency. The peak efficiency occurs at the same ν' that leads to the highest velocity. This can be understood, since at steady-state the consumption rate $b \sim v$, so $\eta \sim v^2/v = v$. Any ν' that generates a peak in v will also generate a peak in efficiency for a fixed a_{tot}. Figure 2.4B shows how the efficiency varies with changing substrate concentration, a_{tot}, for a fixed burn rate constant , ν'. For a given ν', there is an optimal substrate concentration, a_{tot}, that leads to the highest efficiency. Since the consumption rate scales with a_{tot}, the efficiency scales with $\frac{1}{a_{\text{tot}}}$, so a substrate concentration that is too large will lead to inefficient operation.

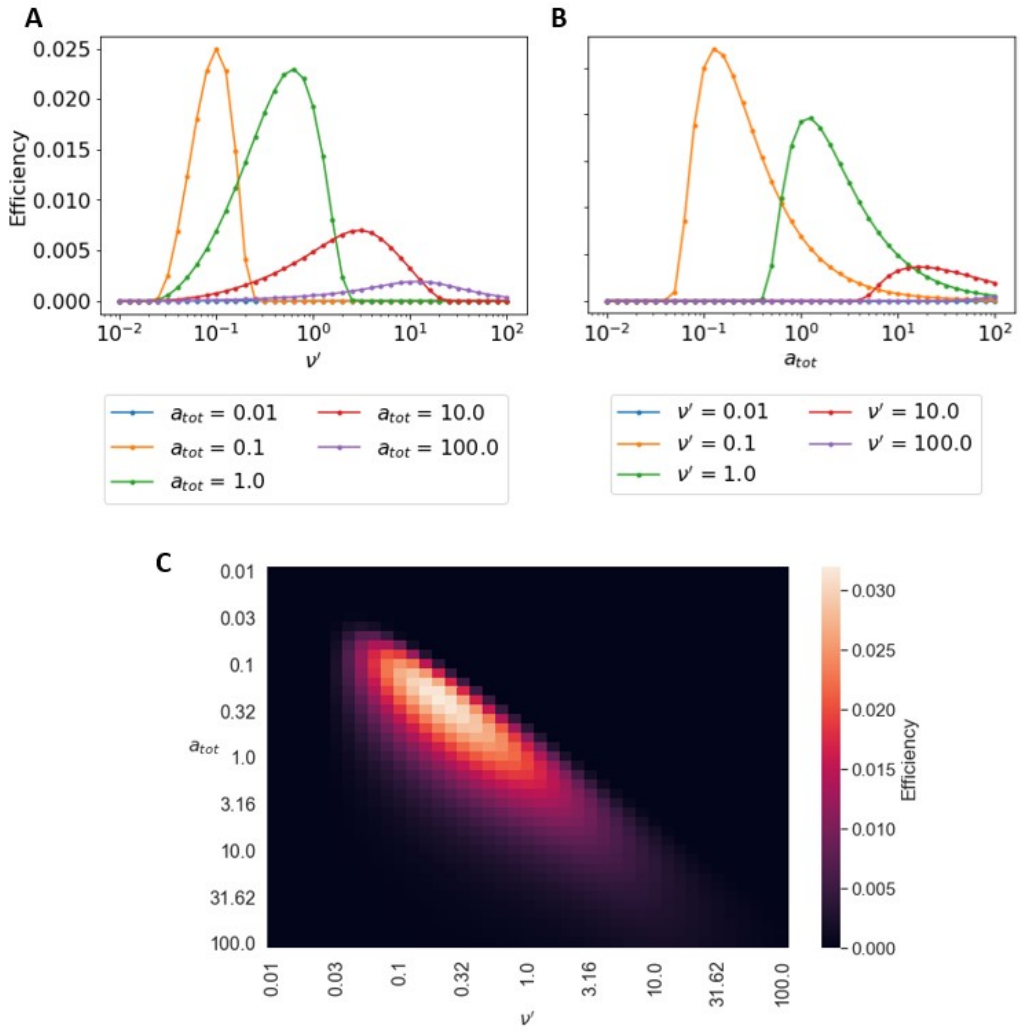

Figure 2.4: **Dependence of efficiency on system parameters with no complex unbinding.** (A) Stokes efficiency of system as a function of burn rate constant , ν' at different substrate concentrations a_{tot}. Given a_{tot} ν' may be adjusted to provide maximum efficiency. (B) Efficiency as a function of a_{tot} at different burn rate constants ν'. (C) Heat map of the efficiency as a function of a_{tot} and ν'. There is an optimal a_{tot} and ν' that lead to the highest efficiency given a fixed amount of input chemical energy, Δg. In all of the above calculations, $\omega' = 0$, $k'_{\text{off}} = K = 0.01$, $\Delta g = 15$.

In Figure 2.4C, I plot the efficiencies as a function of ν' and a_{tot} as a heat map. Although one can continue to increase the steady-state speed of the hub by increasing a_{tot} and ν', the same is not true for efficiency. Indeed for a given substrate binding chemistry, there is is an optimal value of a_{tot} and ν' that leads to the greatest efficiency. When operating at high speeds, the hub is burning relatively more substrate, leading to lower efficiencies. At the opposite end of low a_{tot} and ν', the hub is effectively stalled, though it continues to burn substrate (due to rebinding of substrate), yielding zero efficiency. At optimal ν' and

a_{tot}, the hub moves fast enough to maintain a substrate gradient but slow enough that the consumption rate remains small.

I now show how the unbinding rate constant of the substrate, k'_{off}, affects efficiency. The effects of substrate turnover, from the surface to the buffer and back, decrease with k'_{off}. A small k'_{off} means that little surface-bound substrate is liberated into the buffer, and with low concentrations of free substrate in the buffer, substrate rebinding is slow. This effect is also seen mathematically as every rebinding term in Equation (2.6) scales with k'_{off}. In Figure 2.5, I show that the overall efficiency of the motor decreases with greater k'_{off}. This is due to a larger remainder caused by a high substrate turnover. A larger remainder creates a large amount of negative work on the motor since a large concentration of surface-bound substrate leftover at the back of the hub leads to an increase in a force pulling against the motion of the motor. This leads to a lower efficiency since substrate is still consumed but unidirectional motion is opposed. In addition to this, the optimal efficiency shifts to lower values of v' and a_{tot} as k'_{off} decreases. Because there is lower turnover of substrate, each substrate molecule does positive work on the motor, and at low speeds, the hub makes use of every substrate interaction allowing it to be very efficient. When the motor is moving slowly it has time to bind to nearly all the substrate while the substrate is still in front of the motor. For completely irreversible substrate binding (i.e., $k'_{\text{off}} = 0$), our findings show that efficiency increases with decreasing concentration and burn rate constant . I believe this is due to the motor ratcheting high energy fluctuations in a similar manner to the information ratchet presented by Saha et al.[70]. At low velocities our system waits some distance greater than σ from a substrate molecule. Once the substrate passes a specified threshold (i.e. the distance to the hub) the hub makes the observation (by binding to it) and ratchets the high energy fluctuation.

However, at low enough substrate concentrations and burn rate constants, stochastic effects become important which make the assumptions leading to our deterministic formulation problematic. I expect that stochastic effects at low substrate concentrations and burn rate constants would favour diffusive behaviour of the motor, and hence inefficient operation. If the motor's motion is diffusive it will still consume energy but will have a net displacement of zero. For large k'_{off} (e.g., $k'_{\text{off}} = 0.1$), there is high substrate turnover leading to a rapid filling in of the wake, and so the hub must operate at larger a_{tot} and v' in order to move. However, this comes at the cost of being less efficient.

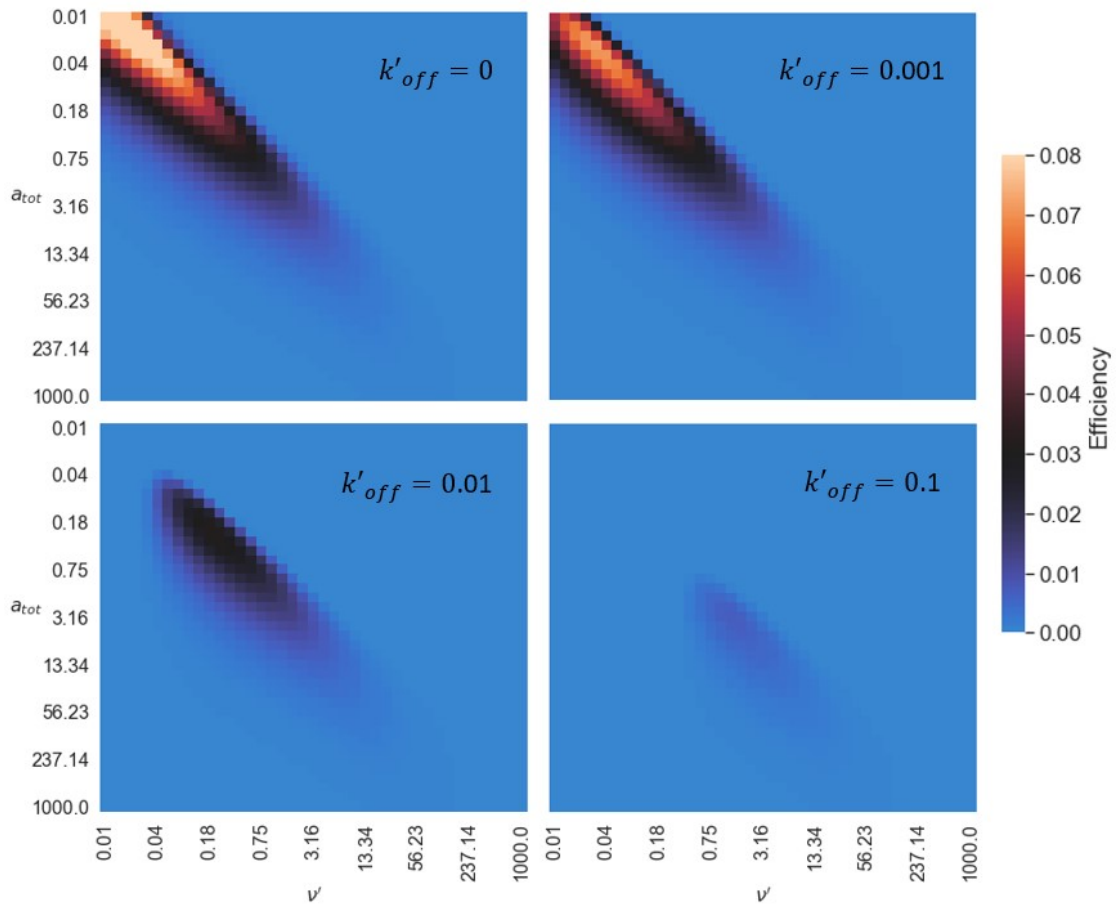

Figure 2.5: **Effects of rebinding on efficiency.** Efficiency heat maps for different k'_{off}. In all of the above calculations, $\omega' = 0$, $\Delta g = 15$.

Motor Efficiency Including Force-Dependent Complex Dissociation

I now consider the situation where substrate bound to the complex can dissociate before being burned. This is parameterized by a complex unbinding rate constant , ω'. I will also consider that this dissociation is force-dependent due to the pulling force acting on the substrate-hub bond. This is parameterized by δ', the distance between the bound and unbound states of the substrate to the hub ($\delta' = 0$ corresponds to no force dependence). In Figure 2.6A, I show the normalized velocity of the hub, with a fixed burn rate constant $\nu' = 1.0$, as a function of unbinding rate at several different substrate concentrations, a_{tot}. The velocities are normalized by the largest velocity for each curve. The plot shows some curves starting just below 1.0, this is a result of some curves depending more on ω' than others. At high substrate concentrations the velocity stays near the maximal velocity as ω' increases while it drops away more rapidly for smaller a_{tot}. However, the overall effect of including dissociation of substrate from the hub is to reduce the velocity of the motor. In Figure 2.6B, the normalized consumption rate is plotted as a function of ω'. Not surprisingly,

the consumption rate goes down with increasing unbinding rate constant . It decreases most rapidly at lower values of substrate concentration. Figure 2.6C shows the resulting Stokes efficiency as a function of ω'. At low substrate concentrations the peak efficiency occurs when $\omega' = 0$. Interestingly, at higher substrate concentrations, the peak efficiency is at $\omega' \neq 0$. Thus, having some amount of complex dissociation back into free substrate leads to more efficient motor operation. I can make sense of this by recalling that at higher a_{tot} the consumption rate decreases while little change in velocity occurs. Figure 2.6D shows the effect of including force-dependent dissociation. For a fixed a_{tot} and ν', increasing δ' simply shifts the efficiency curve. At larger δ', the force acting on the hub leads to a greater overall unbinding rate. The result is that efficiency is maximized at a lower overall unbinding rates, ω', when force is included.

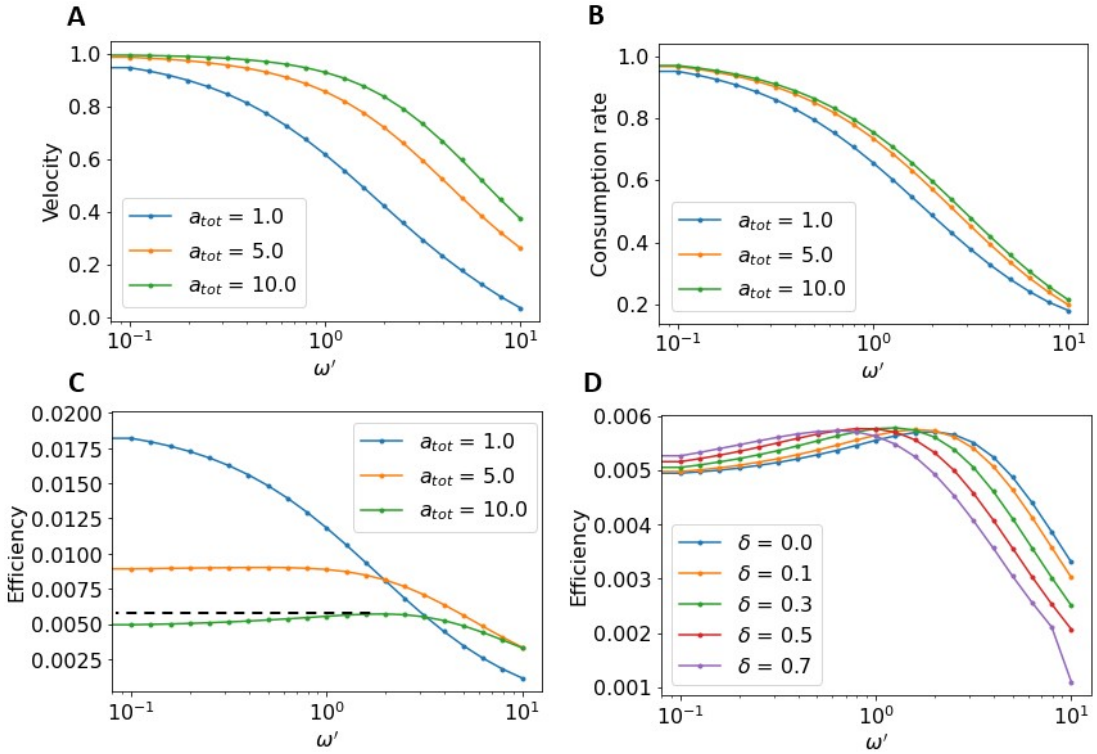

Figure 2.6: **Effects of complex unbinding on efficiency.** (A) The normalized velocity as a function of ω'. Velocities normalized by the maximum velocity for a given a_{tot}. (B) The normalized consumption rate as a function of ω'. (In A,B some curves approach 1 slowly). (C) The absolute efficiency as a function of ω' at different a_{tot}. At lower substrate concentrations the maximal efficiency occurs when there is no complex unbinding (i.e., $\omega' = 0$). At higher substrate concentration (i.e., $a_{\text{tot}} = 10$) the optimal efficiency occurs at a non-zero unbinding rate constant . For calculations in (A–C), $\delta' = 0$. (D) The efficiency as a function of ω' at different δ'. For larger δ' the optimal ω' is greater. δ' makes no significant difference in the global maximal efficiency of the motor. For calculations in D, $a_{\text{tot}} = 10$. In all of the above calculations, $\nu' = 1$, $k'_{\text{off}} = K = 0.01$, $\Delta g = 15$.

2.4 Discussion

In this chapter, I explored the efficiency of a polyvalent motor hub acting as a burnt-bridge ratchet using a minimal deterministic model for its chemistry and dynamics. Through computational simulations I mapped out the dependence of the hub's velocity and consumption rate as a function of the total substrate concentration, a_{tot} and burn rate constant , ν'. I found that the motor exhibited steady-state ballistic motion in regions of the parameter space and stalling in others. As found in previous studies, for a fixed amount of substrate, there is an optimal burn rate constant , ν', that leads to the highest motor velocity. I found that at a fixed burn rate constant , ν', increasing a_{tot} led to an increase in velocity up to a point where it saturated. This was due to the increasing concentration of unburnt substrate left behind the hub that could balance any increases in force from the front. Using the speed and consumption rate, I found that the maximal efficiency for a given a_{tot} is located at the maximal velocity while the maximal efficiency for a given ν' is located well below its maximal speed. This is because the consumption rate scales with a_{tot} and therefore the efficiency scales with the $\frac{1}{a_{\text{tot}}}$. As v saturates with increasing substrate concentration, the efficiency stops increasing and is dominated by the large a_{tot} and begins to decrease.

I also looked at the effect of varying k'_{off} on the efficiency. I found that the maximal efficiency decreases with greater k'_{off} due to the negative work that results from large amounts of substrate turnover. A large substrate turnover allows the system to return to the steady-state substrate concentration faster. I also saw that for k'_{off} that discourages substrate turnover, the efficiency global maximum was located at low a_{tot} with correspondingly low ν'. In the low turnover regime, optimal efficiency is higher at low velocities as a result of efficiency scaling as $\frac{1}{a_{\text{tot}}}$; despite the decreased hub velocity, the decreased a_{tot} dominates the efficiency. Furthermore, the optimal a_{tot} and ν' were much higher when substrate turnover became significant. When substrate turnover is significant, the motor requires enough substrate to allow it to move faster and outpace the substrate rebinding.

Interestingly, when zero substrate rebinding occurred, the efficiency increased monotonically for lower velocities. As the motor slows, the concentration profile of bound complex shifts further from the motor until it is forced to make displacements of greater than σ in order to interact with the hub. When this happens, energy greater than the mean energy of the buffer is provided to the motor resulting in high efficiencies. However, this energy may be accounted for by including the exchange of information and the increase in entropy that results from the cleaving of substrate from the surface.

Finally, I saw that in some regions of the ν'/a_{tot} parameter space that some degree of substrate unbinding may provide local improvement to efficiency. It was found that the bound complex unbinding rate constant , ω', could improve efficiency by decreasing the burn rate constant . I also noted that the distance between the bound complex and surface-bound states , δ', shifts the optimal ω'; δ' should be accounted for when optimizing

efficiency. The strength of the bound complex bond can be decreased in the case of the rolling DNA-RNA motor by Blanchard et al. by shortening the binding region in the complimentary DNA-RNA sequences. Such changes could increase *omega*. I expect that molecular motor engineers could make use of some substrate unbinding to improve their motors' efficiency and should not always attempt to remove substrate unbinding.

This work highlights key parameters that can be tuned to optimize the efficiency of synthetic BBR motors. In many cases, the substrate concentration, burn rate constant and force-dependent unbinding rate constant can be controlled by the experimenter. The substrate concentration has been controlled in several previous experiments [19, 43]. In some cases, the burn rate constant may be adjusted by altering the concentration of enzymes selected to catalyze the motor-substrate bonds [43]. The force-dependent unbinding rate constant has been tuned in other experiments by affecting the free energy associated with the binding [19, 38, 43]. Future work can verify these results in vitro and utilize them to optimize motor efficiency. The testing of in vivo systems may also reveal how well tuned living systems are to optimize efficiency and motility.

2.5 Appendix

2.5.1 Analytic approximation

While full numerical simulations are required to elicit the system dynamics, it is possible, under some assumptions, to calculate the steady-state velocity and, to high accuracy, approximate the efficiency for a given ν' and a_{tot}. First, I assume that there is zero substrate rebinding to the surface; once it has been burnt by the motor, free substrate remains in the buffer indefinitely (i.e. $k'_{\text{off}} = K = 0$). Second, I assume that there is zero unbinding, $\omega = 0$. Under these assumptions the dimensionless, governing equations become

$$\frac{dx_h}{d\tau} = -\int (x_h - x) a_c(x)\, dx\,, \tag{2.9}$$

$$\frac{da_c(x)}{d\tau} = e^{-\frac{(x-x_h)^2}{2}} a_s(x) - \nu' a_c(x)\,, \tag{2.10}$$

$$\frac{da_s(x)}{d\tau} = -e^{-\frac{(x-x_h)^2}{2}} a_s(x)\,. \tag{2.11}$$

At steady-state the hub's position is moving with a constant speed and satisfies $x_h = v\tau$. So at time $\tau = 0$, the hub will be at position $x_h = 0$. I will consider that it achieved steady-state at some long time in the past $\tau = -\infty$ and has been propagating along with constant speed since then. This will allow us to integrate and solve for the steady concentration profile for $a_s^*(x)$ and $a_c^*(x)$, for a given set of parameters ν' and a_{tot}, and our unknown steady-state speed v. I can then substitute these steady-state profiles into Equation (2.9)

which gives a transcendental equation for the speed v. Setting $x_h = v\tau$ into Equation (2.11) gives

$$\frac{da_s^*(x)}{d\tau'} = -e^{-\frac{1}{2}(v\tau'-x)^2} a_s^*(x)\,. \tag{2.12}$$

Rearranging and then integrating from $\tau' = -\infty$ to τ (where I start with $a_s(x, -\infty) = a_{\text{tot}}$) I get that the steady-state profile at time τ is

$$a_s^*(x,\tau) = a_{\text{tot}} \exp\left[\sqrt{\frac{\pi}{2}} \frac{\text{erf}(\frac{x-v\tau}{\sqrt{2}}) - 1}{v}\right]. \tag{2.13}$$

This then gets substituted into Equation (2.10) and I integrate from $\tau = -\infty$ up to $\tau = 0$ so that I have the steady-state complex concentration with the hub at position $x_h = 0$. The solution to Equation (2.10) does not have any closed form solution, but may be written in integral form as

$$a_c^*(x) = \int_{-\infty}^{0} d\tau\, e^{\nu\tau} e^{-\frac{1}{2}(x-v\tau)^2} a_s^*(x,\tau)\,. \tag{2.14}$$

So,

$$a_c^*(x) = a_{\text{tot}} \int_{-\infty}^{0} d\tau\, e^{\nu\tau} e^{-\frac{1}{2}(x-v\tau)^2} \exp\left[\sqrt{\frac{\pi}{2}} \frac{\text{erf}(\frac{x-v\tau}{\sqrt{2}}) - 1}{v}\right]. \tag{2.15}$$

Lastly, I integrate Equation (2.4) using the above $a_c^*(x)$, yielding a transcendental equation for the steady-state velocity,

$$v - \int_{-\infty}^{\infty} dx\, x\, a_c^*(x) = 0\,. \tag{2.16}$$

The roots of the analytic transcendental equation (2.16) were solved using `brentq` from `scipy.optimize`.

Figure 2.7(A,D) shows the analytic approximation (lines) and simulated (crosses) steady-state velocity as a function of burn rate at a given substrate concentration. The two results are in agreement for velocities greater than ~ 0.01 (marked as a black line). I believe the two results diverge for velocities below this threshold due to the inability for simulations to run sufficiently long to reach steady-state.

The consumption rate may also be estimated by making the approximation that all substrate is consumed as the hub passes over it. If the hub has reached steady-state velocity it then consumes a set amount of substrate in a period of time as shown in Figure 2.8. The total substrate consumed in time t is given by the light blue region,

$$bt = vta_{\text{tot}}\,,$$

therefore,

$$b = va_{\text{tot}}\,. \tag{2.17}$$

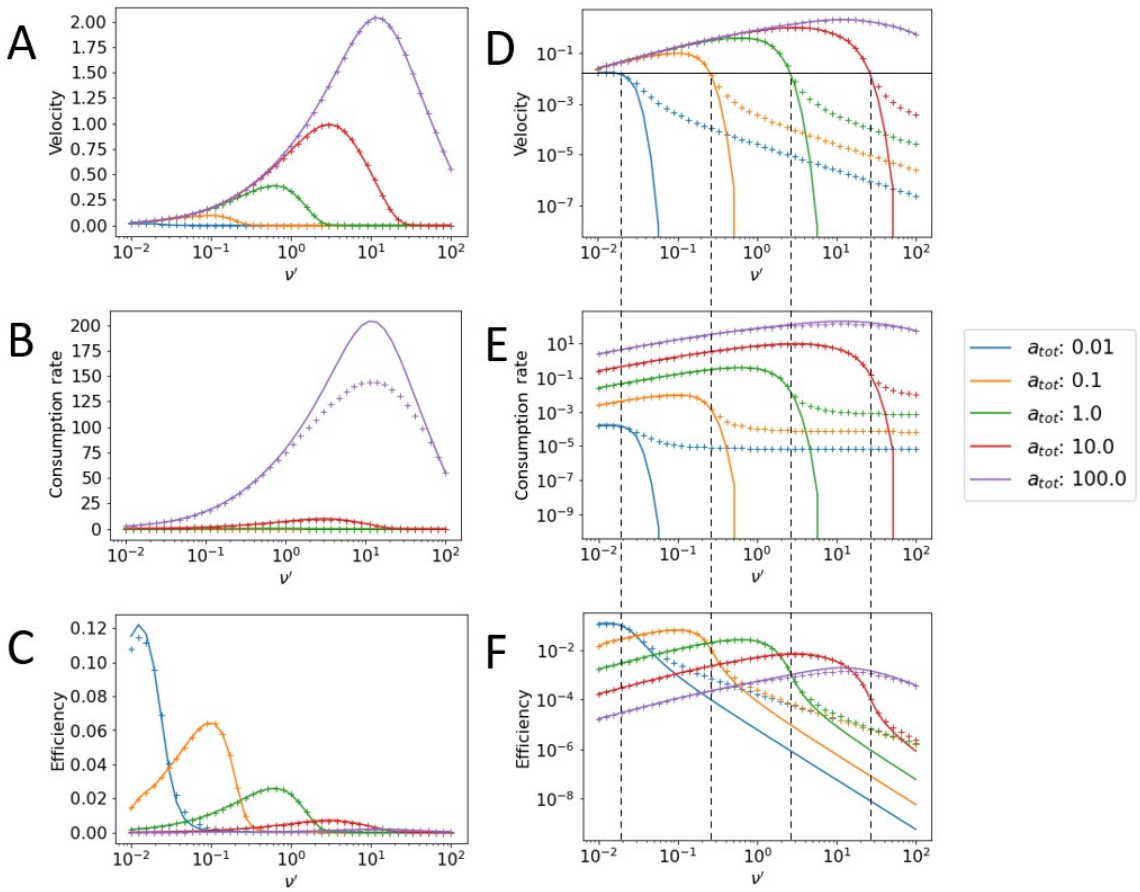

Figure 2.7: **Comparison of analytic and numerical velocities and efficiencies** Two columns represent the same information with linear scale on the right and log scale on the left. (A,D) Steady-state velocity as a function of ν'. For velocities greater than ~ 0.01 (horizontal black line) the approximation holds. (B, E) The consumption rate as a function of ν'. The approximation fails when the ratio of a_{tot} to ν' becomes too small. (C,F) The Stokes efficiency as function of ν'. The vertical dashed lines show that the consumption rate and efficiency approximations breakdown at the same ν' that the velocity breaksdown. Lines represent approximated analytic values, crosses represent simulated values.

Figure 2.7(B,E) show the approximated consumption rate (lines) and the simulated consumption rates (crosses). The approximation does not perform well for high substrate concentrations; this is due to the remainder of unconsumed substrate left behind the hub violating the key assumption that all substrate in the path of the hub is consumed. The consumption rate approximation also breaks down for regions of the parameter space where the analytic velocity approximation began to diverge from the simulated results. This is due to the dependence of the consumption rate on the velocity ($b = va_{\text{tot}}$).

With both the steady-state and consumption rates approximated, I may also approximate the efficiency. Since the efficiency is given by

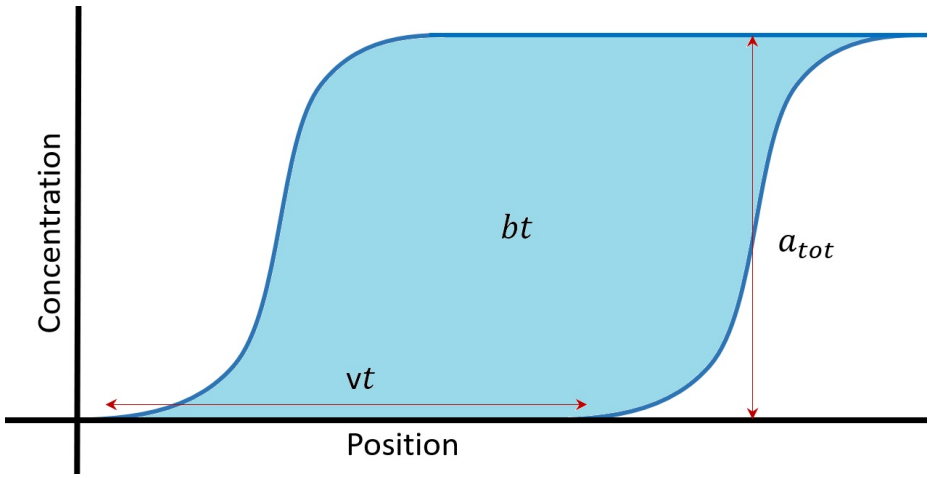

Figure 2.8: **Consumption rate approximation.** The total substrate consumed in time ,t, is given by the light blue region.

$$\eta = \frac{v^2}{\Delta g b},$$

I substitute the expression for the approximated consumption rate and get

$$\eta = \frac{v}{\Delta g a_{\text{tot}}}.$$

I plot the approximated (lines) and simulated (crosses) efficiencies in Figure 2.7(C,F). Of course, the approximated values diverge from the simulated values for the same regions of the parameter space that the velocities and consumption rates diverge from the simulated values.

2.5.2 Steady-state concentration

Here, I look at the full derivation for the steady-state surface-bound concentration for a system with non-zero substrate rebinding. Assuming the motor is small compared to the system (i.e. $A_{\text{tot}} = A_s + A_f$), I can approximate the dynamics of the surface-bound substrate as

$$\frac{dA_s(X)}{dt} \simeq k_{\text{on}} A_f(X) - k_{\text{off}} A_s(X) = k_{\text{on}}(a_{\text{tot}} - A_s(X)) - k_{\text{off}} A_s(X).$$

At steady-state, $\frac{dA_s^*(X)}{dt} = 0 = k_{\text{on}}(A_{\text{tot}} - A_s^*(X)) - k_{\text{off}} A_s^*(X)$, or

$$A_s^*(X) = \frac{A_{\text{tot}}}{(1 + k_{\text{off}}/k_{\text{on}})}.$$

So the rebinding rate would be

$$k_{\text{on}} A_f = k_{\text{on}}(A_{\text{tot}} - A_s^*(X)) = \frac{k_{\text{off}}}{(1 + k_{\text{off}}/k_{\text{on}})} A_{\text{tot}} \,.$$

2.5.3 Consumption rate scaling when rebinding is included

In the case that substrate may rebind to the surface, the approximation made in equation (2.17) does not hold. However, I still wish to confirm that the velocity of the hub roughly scales with consumption rate . Figure 2.9 demonstrates that $b \sim v$ is a reasonable approximation even when substrate rebinding occurs.

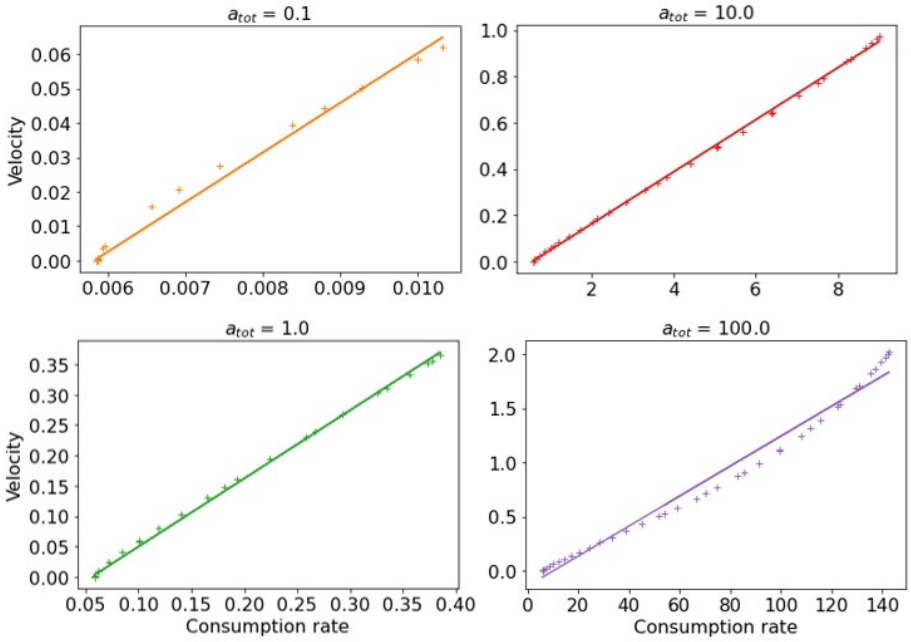

Figure 2.9: **Velocity scaling with consumption rate**. Velocity v as a function of consumption rate b for different a_{tot}. Crosses represent simulated results. Lines represent a linear fitting. At substrate concentrations of less than 0.1 the hub was stalled leading to velocities below computational tolerance.

Chapter 3

Characterising efficiency and motility of a diffusing polyvalent motor hub

3.1 Introduction

The previous chapter demonstrated that efficiencies could be optimized provided that there was some substrate rebinding to the surface. Otherwise, the efficiencies were monotonically increasing for regions of parameter space that generate low velocities. I discussed that the deterministic model may operate in a similar manner to an information ratchet in which high energy fluctuations are ratcheted by a series of observations by the motor and substrate. If this ratcheting of high energy fluctuations is ignored it appeared that the motor could exceed an efficiency of one when the motor moves slow enough and no substrate rebinding took place. I now look at a stochastic model in which the motor diffusion is considered. Where at low concentrations or weak driving force, the system may be dominated by diffusion and therefore have a low efficiency.

In this chapter, I investigate a diffusing, spherical, polyvalent motor hub that interacts with substrate by binding and catalysing substrate dissociation. Due to the stochastic nature of the model, several features are ignored to allow for model simplification and tractable computation time. Namely, surface-bound substrate no longer naturally dissociates to the buffer and free substrate does not rebind to the surface. These assumptions are reasonable for in vitro experiments [43, 74, 101]. Additionally, I assume that once the motor is bound to substrate it remains bound until the substrate is burned and moves into the buffer. All unbinding occurs as a result of motor catalysis.

I find that the motility and efficiency of the motor are characterised by its diffusion coefficient (which depends on its size and the viscosity of the fluid). In addition to this, the substrate burn rate constant and initial substrate concentration influence the motility and efficiency of the motor. I map out the parameter space for the steady-state velocity, consumption rate and efficiency. I find that hub velocity increases as the hub gets smaller, and has a correspondingly smaller drag coefficient. However, the same is not true for the

efficiency. In line with previous results, I find that the efficiency is greatest at low velocities and that the efficiency continues to increase (with no apparent bound) for lower and lower velocities. Trajectories are most ballistic when the drag coefficient is small. Lastly, I note that the length of simulation time has little effect on the characteristic motion and velocity of the motor. The motor is either highly processive or it is highly diffusive. There exists very little intermediate behavior.

3.2 Model and methods

Our model consists of a diffusing motor hub interacting with elastic substrate bound to a one-dimensional track. The motor binds to the substrate, experiences an elastic restoring force and then catalyzes the removal of substrate. During this process the substrate exists in one of three states: surface-bound, bound complex or free in the buffer (Figure 3.1A). The surface-bound and bound complex substrate concentrations at position X are denoted by $A_s(X)$ and $A_c(X)$ respectively (Figure 3.1B).

The driving force from the bound complex is the same as in Chapter 2, namely,

$$F = \int -k(X_h - X)A_c(X)dX\,,$$

In addition to the force from the bound complex, the motor feels random forces from the thermal energy of the buffer. These forces scale in proportion to the diffusion coefficient of the hub given by

$$D = \frac{k_B T}{\gamma}\,.$$

γ is the drag coefficient, which for a spherical particle is $\gamma = 6\pi\eta' R$, where η' is the viscosity of the buffer and R is the radius of the hub.

I simulate the dynamics of the hub in the overdamped regime using the Langevin equation,

$$\gamma\frac{dX_h}{dt} = -\int k(X_h - X)A_c(X)\,dX + \sqrt{2\gamma k_B T}R(t)\,, \tag{3.1}$$

where $R(t)$ is an uncorrelated Gaussian process satisfying $\langle R(t)\rangle = 0$ and $\langle R(t)R(t')\rangle = \delta(t-t')$.

The equations determining the rate of change of the bound complex and the surface-bound substrate are similar to those in Chapter 2, except that they do not consider substrate rebinding or complex dissociation. The chemical kinetic equations we consider are

$$\frac{dA_c(X)}{dt} = re^{-\frac{\beta}{2}k(X-X_h)^2}A_s(X) - \nu A_c(X)\,, \tag{3.2}$$

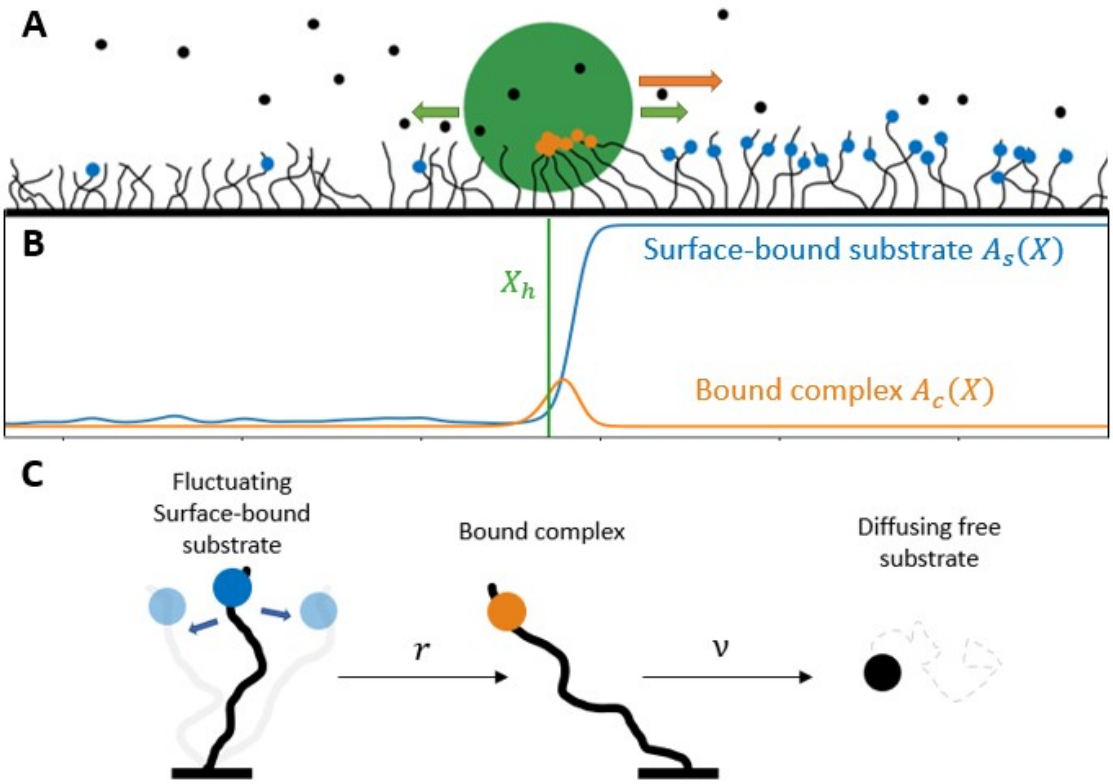

Figure 3.1: **Model schematic.** (A) The motor hub (green) interacts with surface-bound substrate (blue), shifting substrate to the bound complex state (orange) which is eventually burnt and freed to the buffer (black). The hub is driven by random unbiased diffusive forces (green arrows) and a net driving force (orange arrow). (B) Example surface-bound and bound complex substrate concentrations and the location of the hub at a single point in time. The motor hub is currently moving right. (C) Schematic of state transitions and associated rates. All reactions are considered irreversible.

$$\frac{dA_s(X)}{dt} = -re^{-\frac{\beta}{2}k(X-X_h)^2}A_s(X)\,. \tag{3.3}$$

Here I non-dimensionalize the above equations similar to what was done in Chapter 2, but with a different definition of the reference concentration,

$$a_0 = \frac{1}{\sigma}\,,$$

where σ is the fluctuation of the surface-bound substrate. Additionally, D is non-dimensionalised as

$$D = D'D_0\,,$$

where I define a reference diffusion coefficient, $D_0 = r\sigma^2$. Where r is the binding rate, and σ is the characteristic fluctuation length. These substitutions lead to the following dimensionless equations,

$$\frac{dx_h}{d\tau} = -D' \int (x_h - x) a_c(x)\, dx + \sqrt{2D'}\zeta(\tau)\,, \tag{3.4}$$

$$\frac{da_c(x)}{d\tau} = e^{-\frac{(x-x_h)^2}{2}} a_s(x) - \nu' a_c(x)\,, \tag{3.5}$$

$$\frac{da_s(x)}{d\tau} = -e^{-\frac{(x-x_h)^2}{2}} a_s(x)\,, \tag{3.6}$$

where $\nu' = \frac{\nu}{r}$. Here the force term $(-D' \int (x_h - x) a_c(x)\, dx)$ scales with D'.

3.2.1 Efficiency

Since our motor operates in a similar environment as in Chapter 2 I use the Stokes efficiency as before. Now however, the motion is stochastic and I must use an ensemble average velocity $\langle V \rangle$ and an ensemble average consumption rate $\langle B \rangle = \Delta G \nu' \langle \int A_c(X) dX \rangle$,

$$\eta = \frac{\gamma \langle V \rangle^2}{\langle B \rangle}\,.$$

Non-dimensionalising as before we get

$$\eta = \frac{\gamma \sigma^2 r^2 \langle v \rangle^2}{\Delta g k_B T r \nu' \langle \int a_c(x) dx \rangle}\,,$$

where $\frac{\gamma}{k_B T} = \frac{1}{D}$, which leads to

$$\eta = \frac{\sigma^2 r \langle v \rangle^2}{\Delta g D \nu' \langle \int a_c(x) dx \rangle}\,.$$

Then setting $D = D' D_0$ we get

$$\eta = \frac{1}{D' \Delta g} \frac{\langle v \rangle^2}{\langle b \rangle}\,. \tag{3.7}$$

It should be noted that the efficiency is explicitly inversely proportional to the diffusion coefficient. This can be understood as an increase in diffusion coefficient leads to reduced viscous drag. Since the definition of the Stokes efficiency has the work done by viscous drag in the numerator, a reduced viscous drag leads to lower efficiency. So while the hub may move faster with a greater diffusion coefficient, it is also doing less work on its environment for a given displacement. With this in mind, it is unclear whether a large or small diffusion coefficient will lead to the greatest efficiency.

The nondimensionalised Stochastic differential equations (SDEs) were solved using Euler's method with fixed time step of $d\tau = 0.001$. Due to the stochastic nature of the SDEs, 30 runs were simulated for each point in parameter space for a time of $\tau_{\max}$. In order to compute the velocity and limit the noise to signal ratio, the values of the force term were averaged for the last $10 - 20\%$ of each trajectory and then each of these time-averages was used to compute the ensemble average velocity. I justify the use of only the force term to compute the velocity as the diffusive term will simply provide unbiased noise and not affect the velocities over long time periods. The ensemble average consumption was calculated using the time-average consumption rate over the same period that was used to calculated the time-average velocities. These were averaged over the ensemble of trajectories to get the ensemble average consumption rate.

I calculated the mean squared displacement by summing the square of the displacements over the 30 trajectories and dividing by the total number of trajectories. To avoid transient motion at the beginning of each simulation, the MSD from the last $10 - 20\%$ of each run is used. Once the transient had disappeared, I set the location of the hub at each trajectory to be zero, and then calculated the MSD from this point over the last $10 - 20\%$ of the run.

The motion of a stochastic particle may be characterised by fitting a power law to the MSD, $\langle x^2 \rangle = A\tau^{\alpha}$, where α is the anomalous diffusion exponent [74]. The value of α determines the characteristic motion of the ensemble, where sub-diffusive, diffusive and super-diffusive motion is given by $\alpha < 1$, $\alpha = 1$ and $\alpha > 1$, and ballistic motion is characterised by $\alpha = 2$ [102, 103]. I use `curve_fit` from `scipy` for fitting the power law to the MSD curves.

3.3 Results

Here I present the results of our stochastic model for a polyvalent hub with diffusion coefficient, D', on a substrate with total substrate concentration, a_{tot}, and with the hub burning the substrate at a rate constant ν' (see Figure 3.1 for schematic). While D′ represents the dimensionless diffusion constant, it is often more intuitive to consider the effect of a changing drag coefficient. D′ is just the inverse of the drag coefficient so a higher D′ represents a low drag coefficient and vise-versa.

In Figure 3.2(A) I plot the concentration profiles of a representative trajectory at a given D'. For different D' the hub is able to maintain a substrate gradient and move processively over the surface. Figure 3.2(B) shows the ensemble average velocity as a function of time for 30 trajectories at different D'. Noise was reduced by averaging the velocities in bins of $\Delta\tau = 1.0$. The fluctuations in velocity are greatest at high D' and the average steady-state velocity must be determined by time-averaging over long windows of time. For low D' the steady-state velocity is readily apparent. Figure 3.2(C) shows the ensemble average consumption rate as a function of time for particle ensembles with different diffusion

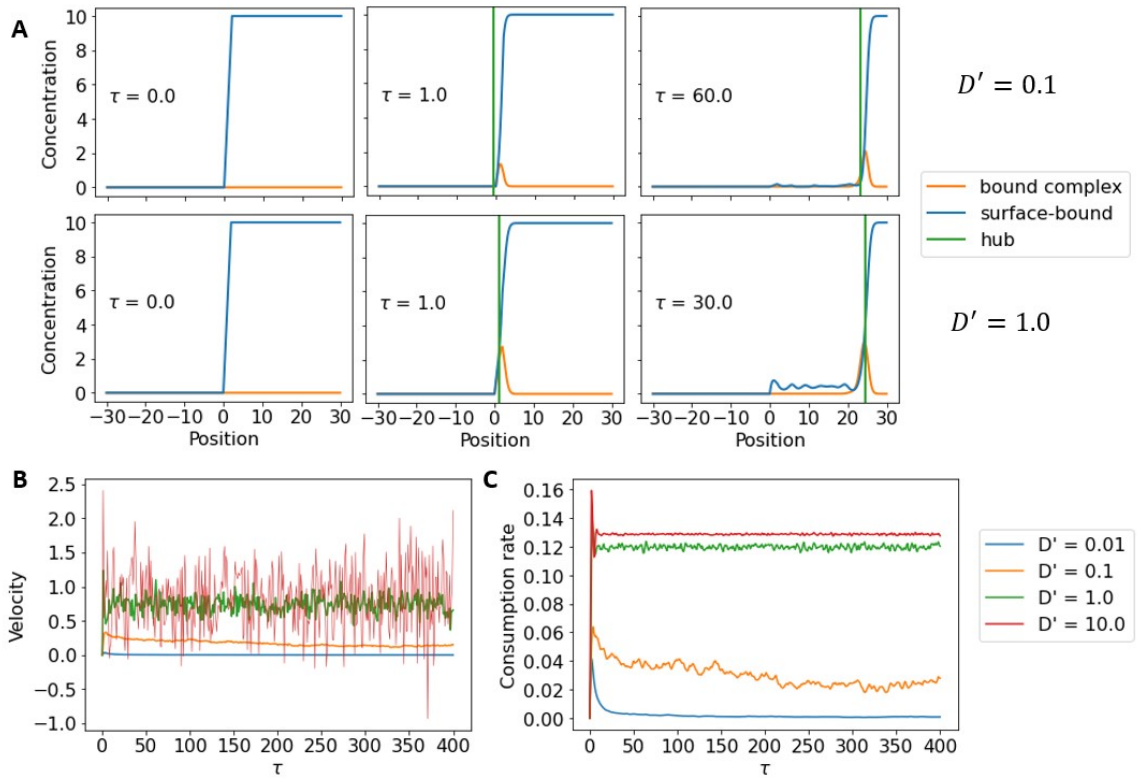

Figure 3.2: **Motor dynamics and reaching steady-state.** (A) Concentration profiles for two trajectories with different diffusion coefficients. The hub is located at $x = 0$ at $\tau = 0$. (B) Ensemble average velocity and (C) consumption rates as a function of time for different diffusion coefficients. For all calculations $a_{\text{tot}} = 10.0$ and $\nu' = 1.0$

coefficients. The ensemble average consumption rate for a motor with a large drag coefficient has low noise and demonstrates the achievement of steady-state early in the trajectory. At low drag coefficients the consumption rate is higher due to the ballistic nature of the average trajectory. The particle is more responsive to forces exerted on it and therefore it spends less time in regions where substrate has already been burnt. Additionally, I find that motors with a high drag coefficient take much longer to achieve steady-state (Figure 3.2(C)).

Figure 3.3 shows the MSD of diffusing particles interacting with substrate in blue and the MSD of freely diffusing particles in red (each simulated with the same $\zeta(\tau)$ for more clear comparison). A particle with a large drag coefficient follows closely to a freely diffusing particle. The force term scales with D' while diffusion scales with $\sqrt{D'}$, so in the limit of small D' the diffusion term dominates. By increasing the size of the particle or the viscosity of the fluid, the particle becomes less inclined to fluctuate, however it also becomes much harder to move the particle by means of the drive force. So larger particles operate more diffusively.

In Figure 3.4(A-C) I map the ensemble average velocity, consumption rate and efficiency over the D'/ν' parameter space. I ensure that the hub has reached or is close to reaching

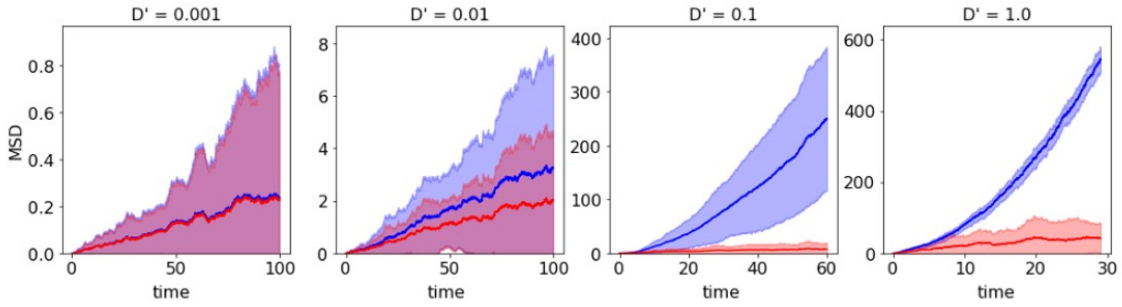

Figure 3.3: **MSD for different diffusion constants** (A) Mean squared displacement over time. Dark Blue: MSD of diffusing particle interacting with substrate; the mean plus and minus standard deviation is shown in light blue. Dark red: MSD of a diffusing particle in the absence of substrate; the mean plus and minus standard deviation is shown in light red. For all calculations $a_{\text{tot}} = 10.0$, $v' = 1.0$ and $N = 30$.

the steady-state velocity by checking the velocity vs. time plots for sample points in the parameter space. For some regions of parameter space, steady-state speed takes longer than is feasible for simulation. The ensemble average velocity is quite noisy as I saw in Figure 3.2, however it is clear that increasing the diffusion constant increases the velocity, and as a result of this, the consumption rate increases. This is due to a larger D' corresponding to a smaller hub and a smaller drag coefficient. At large D' the hub is unlikely to have diffusive motion even though the diffusive term is larger, since the diffusive term only scales with $\sqrt{D'}$ and is dominated by the scaling of the deterministic term that scales with D'.

The optimal velocity and consumption rate for a given D' may be achieved by tuning the burn rate constant . If the burn rate constant is too high the motor will cleave all bonds with the substrate and movement will be entirely governed by the diffusive forces (top right region in Figure 3.6(A-D)). In regions where v' is low (black rectangle in Figure 3.6(A,B)) the hub is predominantly bound to the substrate and has a much smaller effective diffusion coefficient compared to its free diffusion coefficient. In this region, velocity and consumption rates depend only on v'. One can think of this low v' region as behaving similarly to the deterministic model since the hub ignores long term diffusive effects and is predominantly moved by the drive force.

The same is not true for the efficiency however; since the efficiency scales with $\frac{1}{D'}$, the efficiency will be greatest at a low diffusion constant in this region (Figure 3.4(C)). Notably, the efficiency is largest in regions where the hub is moving at smaller velocities. Despite the diffusive term dominating at low D', the motor is able to move processively along the substrate even at low velocities (see Figure 3.4)(D). It is the result of moving processively that leads to efficient operation. As the motors fall off the substrate they begin to have a net zero displacement which results in a low efficiency.

Figure 3.4(D) shows the values of α at several points over the D'/v' parameter space. Trajectories become increasingly ballistic for larger D', which is sensible since the deter-

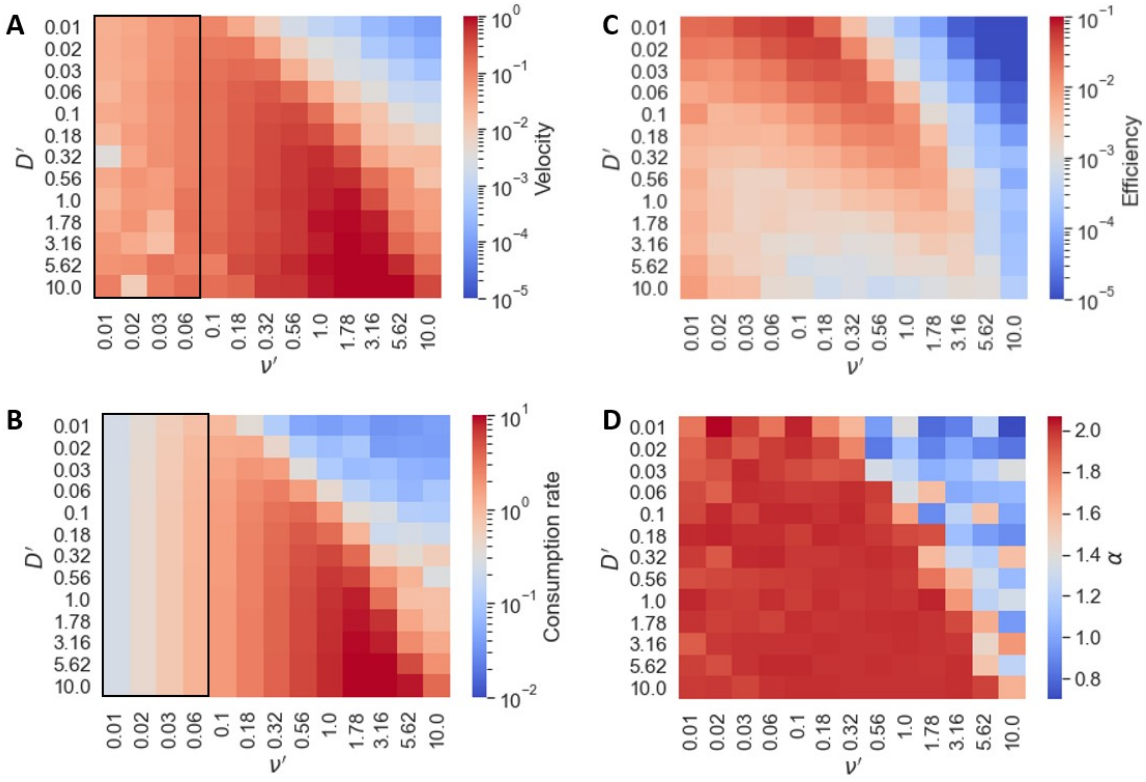

Figure 3.4: **Motor properties in D'/ν' parameter space.** (A) Steady-state velocity as a function of D' and ν'. (B) Consumption rate as a function of D' and ν'. The black rectangle identifies a region where velocity and consumption rates appear roughly independent of the diffusion coefficient. (C) Efficiency as a function of D' and ν'. (D) Anomalous diffusion coefficient as a function of D' and ν'. For all calculations $a_{\text{tot}} = 10.0$, $N = 30$ and $\delta g = 15.0$.

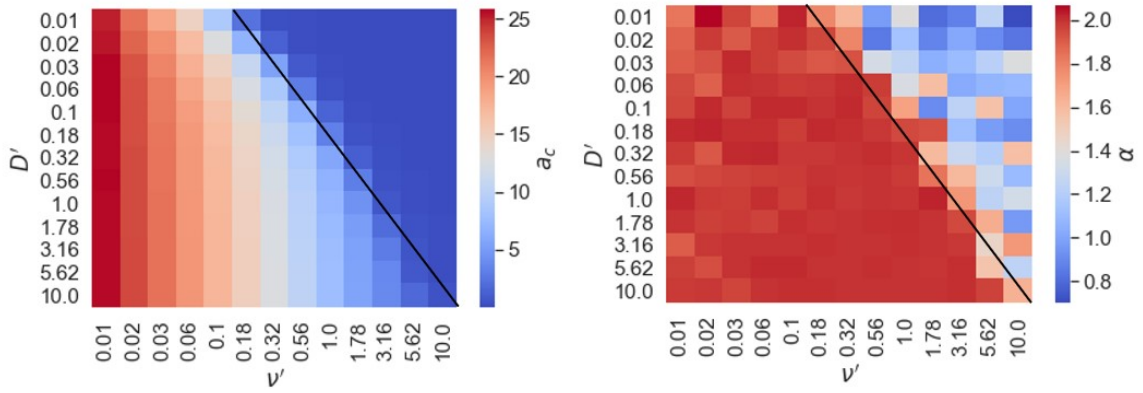

Figure 3.5: **Bound complex concentration for diffusive and ballistic regions.** The total bound complex concentration in the D'/ν' parameter space (Left). Figure 3.4 (Right) include for comparison. The two heat maps have a boundary on the black line. If the particle is diffusive, it is also has a near zero total bound complex concentration.

ministic term dominates in this region. As well, the ballistic nature of the motor may also be tuned by adjusting ν'. If ν' is too large the motor will consume substrate around it too quickly, detach from the surface and begin pure diffusion. Conversely, a burn rate constant that is small will lead to the motor tethering to the surface and effectively negating any long term diffusive effects.

Figure 3.5 shows a comparison of the total bound complex concentration and the anomalous diffusion exponent in the D'/ν' parameter space. To the right of the black line the motor is almost completely detached from the surface since the total concentration of bound complex is near zero. In the same region, the motor is operating diffusively. Thus the motor is either attached and moving ballistically or detached and freely diffusing.

I then look at the a_{tot}/ν' parameter space. Figure 3.6 shows the velocity, consumption rate and efficiencies as a function of a_{tot} and ν'. I see similar effects as a_{tot} increases when compared with an increase in D'. First, the velocity and consumption rates increase (Figure 3.6(A-B)) with a_{tot}. Second, the motor is most efficient when a_{tot} is small (provided ν' is also small) since the motor moves slowly at low concentrations, and importantly, is still processive at low velocities when the burn rate constant is low enough. Third the motor moves more ballistically at high a_{tot} (Figure 3.6(D)) because of the increased binding that occurs when more substrate is available to the hub. Both a_{tot} and D' share these properties since an increase in each results in the scaling of the deterministic term. In contrast to Figure 3.4 however, a_{tot} continues to have an effect on the velocity and consumption rate at low ν'. This is due to the fact that insufficient substrate concentration for the hub to bind limits the hub's ability to tether to the surface. So diffusive motion occurs at low burn rate constants when a_{tot} is also sufficiently low. Figure 3.6(D) further demonstrates this effect as a decrease in burn rate constant leads to ballistic motion. When the substrate concentration is small,

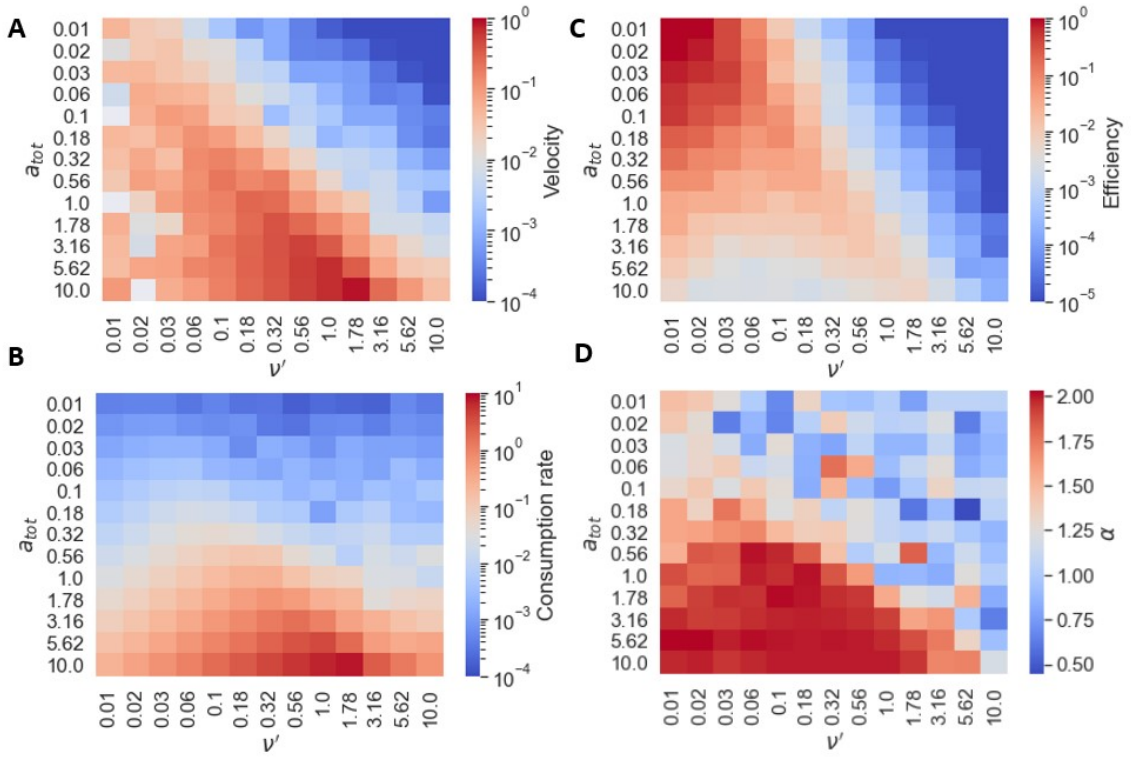

Figure 3.6: **Motor properties in a_{tot}/ν' parameter space.** Velocity (A), consumption rate (B), efficiency (C) and anomalous diffusion exponent (D) as a function of a_{tot} and ν'. For all calculations, $D' = 1.0$, $N = 30$ and $\Delta g = 15.0$.

the diffusive term dominates leading to diffusive motion. However, a low enough ν' may negate this by tethering the motor to the surface.

One might expect that as the length of simulation time increases, a higher fraction of the ensemble will detach from the substrate and begin diffusing (i.e. zero average velocity). If this were the case I would expect the ensemble average velocity to decline with time. In Figure 3.7(A), I show that the motor velocity and characteristic motion have little dependence on the length of time of the simulation. For the length of the simulation, only a small decrease in the ensemble average velocity was observed for some points in parameter space. I also plot the anomalous diffusion exponent as a function of time. In most points in parameter space the system is nearly entirely ballistic or nearly entirely diffusive (with some exceptions at the boundary of the transition) and remains in this state indefinitely. As a bench mark comparison, I take kinesin which is known to be highly processive and takes on the order of 100 steps before falling off the track [104]. As previously stated in Chapter 1, kinesin takes roughly 25-100 steps per second. Indicating that kinesin remains on the track for 1-4s. In our model, time is scaled by the on rate r. So if r is on the order of 0.001 or greater, our system operates at least as processively as kinesin. This demonstrates that the motor moves with either very high or very low processivity. In other words, the entire

ensemble will remain completely attached or completely detached from the surface. This is in agreement with Figure 3.4(D) in which I see a sharp transition at the boundary between the ballistic and diffusive regions, the entire ensemble is either ballistic or diffusive.

3.4 Discussion

In this chapter I explored the efficiency of a polyvalent motor hub acting as a burnt-bridge ratchet using a minimal stochastic model for its chemistry and dynamics. Through computational simulations I mapped out key metrics such as velocity and efficiency as functions of the diffusion coefficient D', total substrate concentration, a_{tot}, burn rate constant , ν' and the total simulation time. The equation of motion for the system consists of two key terms: (i) a deterministic term and (ii) a diffusive term. The deterministic term scales with D' while the diffusive term scales with $\sqrt{D'}$.

I found that a lower drag coefficient lead to more ballistic motion. With a smaller drag coefficient, the ensemble is more greatly influenced by the force of interaction from substrate. Mathematically, this may be understood as the deterministic term increases more quickly with D' than the diffusive term, which only scales with $\sqrt{D'}$. At higher drag coefficient the motor behaved more similarly to a purely diffusing particle since the diffusive term dominates at low D' values. Recall that the diffusion coefficient $D \sim \frac{1}{\gamma}$

I found that the diffusion coefficient had a similar effect on the velocity, consumption rate, efficiency and anomolous diffusion exponent as the substrate concentration. I make sense of this by recalling that an increase of each results in a larger deterministic term with little or no change to the diffusive term. I also noted that a low ν' may completely negative diffusive effects by tethering the motor to the surface (preventing any significant spatial fluctuations over large time windows).

Additionally, I noted that the system operates at highest efficiency when the ensemble moves slowly yet ballistically. Ballistic motion may be achieved at low velocities provided ν' is small enough. If ν' is too large the motor tends to detach from the surface and begins to freely diffuse.

Notably, the efficiency increases monotonically with decreasing hub velocities. Since the motor cannot do more work than it has energy available to it, the work must be a result of something other than conventional energy, namely information. I expect that the extra work done by the motor is a result of the motor observing high energy fluctuations in the substrate and ratcheting these to extract work in a similar manner as described in Chapter 2 and in the work by Saha et al. [70]. This demonstrated that results from our previous study were also applicable for a diffusive motor in that the motor may act similar to an information ratchet that extracts some of its work from the use of information flow [95]. I believe this stochastic model maintains this effect since at low burn rate constants this model may be approximated by the deterministic model presented in Chapter 2. The

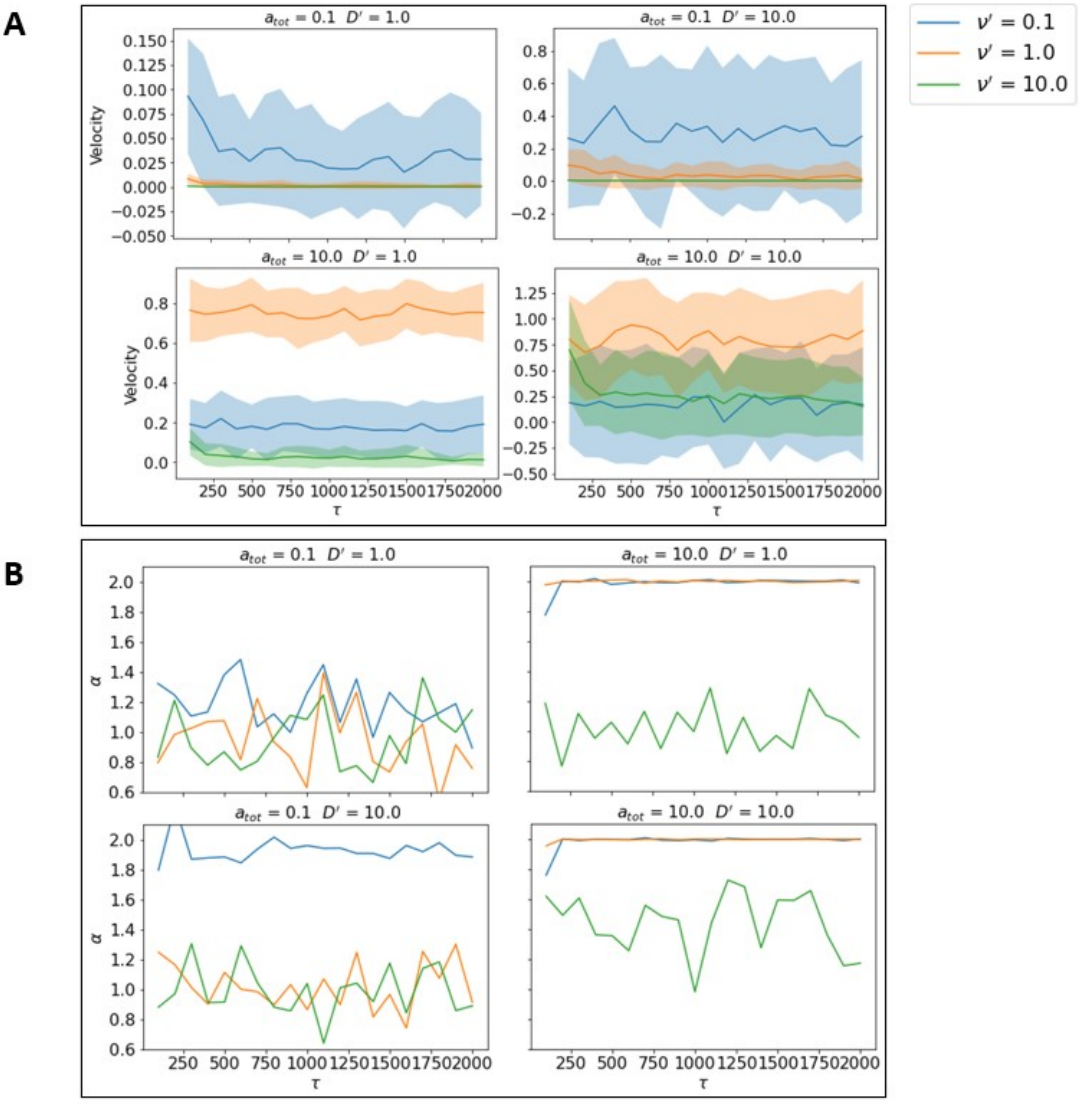

Figure 3.7: **Velocity and characteristic motion time dependence.** (A) The ensemble average velocity (lines) along with the standard deviation (shaded region) as a function of time at different points in parameter space. Mean velocities and standard deviation calculated from bins of length $\tau = 100.0$. (B) The anomalous diffusion exponent of the hub for trajectories of duration τ. 30 trajectories were used for each calculation.

deterministic model is a good approximation at low burn rate constants because, as I saw in this chapter, the motor ignores diffusive effects in the low ν' regime.

Lastly, I found that the motion of the ensemble does not change quickly over time. The system would typically take some time to reach a steady-state velocity and then would remain at this velocity for long periods of time. This means that this type of motor moves with high processivity, once attached to the surface it would remain operating on the surface for a long time.

Chapter 4

Conclusions and Future Work

In this thesis I provided computational models to characterise the motility and efficiency of a motor governed by a burnt-bridge ratchet mechanism. These models were designed to provide experimentally verifiable results and to provide guidance for experimentalistics in optimizing the motility and efficiency of synthetic BBRs.

In Chapter 2, I detailed a deterministic model in which a polyvalent motor hub operates as a BBR. I calculated the Stokes efficiency over the parameter space and found that in the presence of some substrate rebinding, the motor exhibited optimal efficiency at finite substrate concentrations and burn rate constants. However, in the absence of substrate rebinding, the motor efficiency was unbounded. The motor acts similar to the information ratchet created by Saha et al. [70].

I also looked at the effect of unbinding of the substrate. I found that in some regions of parameter space a non-zero unbinding rate constant may improve local efficiency. I discussed how this was a result of a decrease in consumption rate with little decrease in velocity. Lastly, I looked at an analytic approximation for the steady-state velocity, consumption rate and efficiency. I find that for steady-state velocities above a threshold, the approximation holds closely to the simulated results.

In Chapter 3, I extend the model from Chapter 2 by considering the random forces exerted on the hub from the thermal bath. In the absence of substrate interaction the hub would simply diffuse and follow a random walk. In this model I assumed several of the substrate state transition rates are zero for simplicity. I found that the diffusion constant influences the motility, efficiency and processivity of the motor. Due to the scaling of the drag force by the diffusion coefficient, an increased diffusion coefficient leads to more ballistic motion and higher velocities. I also found that the substrate concentration has a similar effect as the diffusion coefficient on the velocity and efficiency. However, the same is not true for the consumption rate as the consumption rate scales with the substrate concentration while this is not always true with the diffusion coefficient.

I also noted that the burn rate constant has a significant impact on the characteristic motion of the motor ensemble. If the burn rate constant is low enough the ensemble will

tether to the surface, where at short time scales the system will undergo tethered diffusive motion and on long time scales the slow chemistry is enough to shuttle the hub along. In this way the motor is able to move ballistically and processively at low velocities provided the burn rate constant is low enough. At high burn rate constants, I found the motor was more likely to be diffusive, which essentially meant that the motor would detach more easily from the surface.

Lastly, I noted that the system was mostly independent of the total time of the simulation. So, either an entire ensemble would be completely processive and remain attached to the surface for long periods of time or they would all completely detach and become diffusive early on. This was corroborated by mapping the anomalous diffusion coefficient over parameter space. The heat map showed a sharp transition between the nearly entirely ballistic regime (low ν' and high D') and the diffusive regime (high ν' and low D').

4.1 Future work

The work in this thesis made several assumptions that may limit the predictive power of the model. First, I assumed that the hub is point-like, in that all binding occurs at its center. This is an especially poor assumption for synthetic BBRs like those created by Blanchard et al. [43]. Second, I assumed that the the hub was able to interact with limitless substrate. This breaks down quickly if substrate concentrations are high or if the hub is small, since there will be more substrate available to bind to the hub than the hub has space available.

4.1.1 Model

Here I present some preliminary work that extends the deterministic model presented in Chapter 2 of this thesis by considering the hub to be of a finite radius, R_h, and to contain finite binding sites, N_h.

I may consider a finite sized hub to be a collection of rigidly connected point-like hubs with limited binding sites. The rate of formation of bound complex for a point-like hub with limited binding sites is

$$\frac{dA_c(X)}{dt} = r\, e^{-\frac{k\beta\Delta r^2}{2}} A_s(X) \frac{N_h(t)}{N_h(0)} - \nu A_c(X)\,, \tag{4.1}$$

where $N_h(t)$ is the number of hub binding sites still available at time, t. When no substrate is bound to a given point on the hub (i.e. $N_h(t) = N_h(0)$, since no substrate is bound to the hub initially) I get back what I had for a point-like hub. And when all binding sites are taken (i.e. $N_h(t) = 0$) no binding occurs. Instead of using $X - X_h$ in the exponent I use a more general Δr, which is the distance that a substrate must stretch to reach a binding site. This depends on the geometry of the hub and the location of the binding site. Δr is a function of the location of the binding site, ϕ, the equilibrium position of the binding

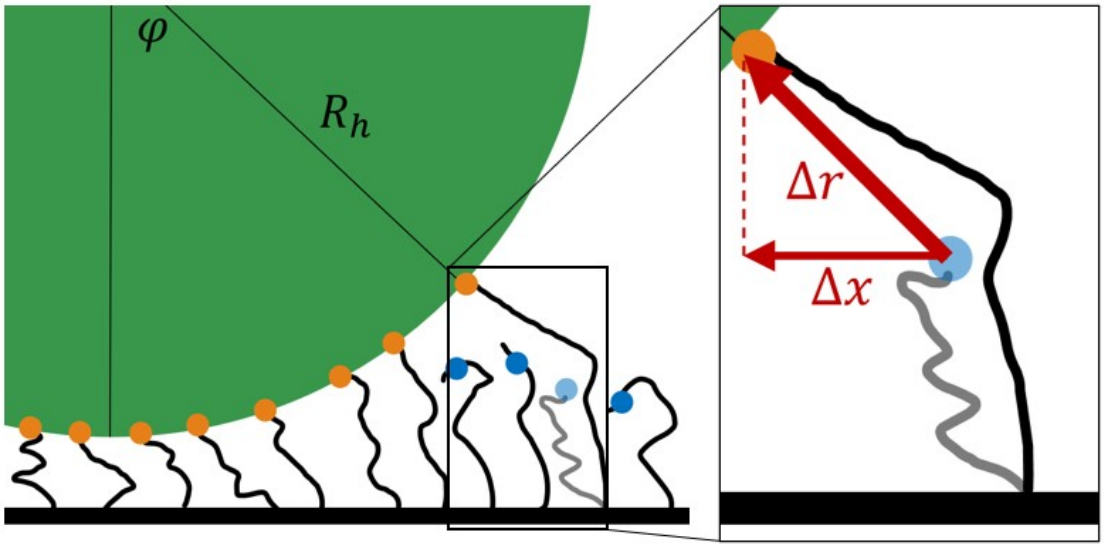

Figure 4.1: **Finite hub model schematic**. (Left) substrate may now bind at any point along the hub surface. (Right) the distance that the substrate stretches now depends on the hub geometry.

substrate, X, and the radius of the hub R_h. When accounting for the curvature of the hub the force term would not change because I am only interested in the horizontal component of force (i.e. $X' - X$, where X' is the location of the hub binding site). However, the rate that the substrate binds to points on the hub will differ since points farther from X_h will have a y component, increasing the distance that the substrate needs to stretch in order to bind (see Figure 4.1). Therefore I may write the equation that describes the distance from a point, X, on the surface to a point, ϕ, on the hub as

$$\Delta r = \sqrt{(X_h + R_h \sin\phi - X)^2 + R_h^2(1 - \cos\phi)^2)}\,.$$

I may also write the extension for the spring in the X-direction as

$$\Delta X = X_h + R_h \sin\phi - X\,.$$

Equation 4.1 may be extended to describe the rate of formation of bound complex between substrate at X and binding sites at ϕ as

$$\frac{dA_c(X,\phi)}{dt} = r\, e^{-\frac{k\beta\Delta r^2}{2}} A_s(X) B_h'(\phi,t) - \nu A_c(X,\phi)\,. \tag{4.2}$$

$A_c(X,\phi)$ describes the concentration of bound complex that connects a point on the surface, located at X, to a point on the hub, located at ϕ. Here $B_h'(\phi,t) = \frac{B_h(\phi,t)}{B_h(\phi,0)}$, where $B_h(\phi,t)$ is the amount of available hub binding sites at a given angle and given time. Since the amount of

bound complex forming is equal to the amount of surface-bound substrate being lost, it follows that

$$\frac{dA_s(X)}{dt} = -\int_{-\pi/2}^{\pi/2} r\, e^{-\frac{k\beta\Delta r^2}{2}} A_s(X) B_h'(\phi,t) d\phi\,. \tag{4.3}$$

The force equation is then

$$\gamma \frac{dX_h}{dt} = -\int\int k\Delta X A_c(X,\phi) dX R_h d\phi\,. \tag{4.4}$$

To determine the $B_h(t)$ I may write

$$B_h(\phi,t) = B_h(\phi,0) - \int A_c(X,\phi) dX\,,$$

since the amount of sites available is just the starting amount less the amount currently used.

A key difference in this model is the inclusion of the scaling of the hub radius on the system dynamics. Equations 4.2, 4.3 and 4.4 are non-dimensionalised using the substitutions

$$X = \sigma x\,,$$

which leads to,

$$\Delta r = \sigma\sqrt{(x_h + R_h'\sin\phi - x)^2 + R_h'^2(1-\cos\phi)^2)} = \sigma\Delta r'\,,$$

$$R_h = \sigma R_h'\,.$$

Additionally,

$$t = \frac{\tau}{r}\,,$$

$$A_i = a_0 a_i\,.$$

The difference from the non-dimensionalisation from Chapter 2 is that I must now leave out R_h from a_0. Since R_h is no longer a set constant but now a parameter that affects the dynamics of the motor, I need to include it in the calculation. So now, $a_0 = \frac{r6\pi\eta'}{k\sigma}$. These substitutions give us the following non-dimensionalised equations,

$$\frac{da_c(x,\phi)}{d\tau} = e^{-\frac{\Delta r'^2}{2}} a_s(x) B_h'(\phi,t) - \nu' a_c(x,\phi)\,, \tag{4.5}$$

$$\frac{da_s(x)}{d\tau} = -\int e^{-\frac{\Delta r'^2}{2}} a_s(x) B_h'(\phi,t) d\phi\,, \tag{4.6}$$

$$\frac{dx_h}{d\tau} = -\int\int \Delta x a_c(x,\phi) dx d\phi \,. \tag{4.7}$$

Notably, the force equation does not depend on the hub radius. This is due to the equal scaling of both the drag coefficient and the force with R_h. Equations 4.5, 4.6, 4.7 were solved with Euler's method with time step of $\Delta\tau = 0.001$.

4.1.2 Efficiency

The efficiency will be the same as in Chapter 2 but with different notation to express the bound complex. The efficiency will be converted from dimension-full quantities,

$$\eta = \frac{\gamma V^2}{\Delta G \nu \int\int A_c dX R_h d\phi},$$

to dimensionless quantities,

$$\eta = \frac{v^2}{\Delta g \nu' \int\int a_c dx d\phi} \,. \tag{4.8}$$

4.1.3 Preliminary results

Figure 4.2 shows influence of the hub radius and the number of binding sites on the steady-state distribution of $B_h(\phi,\tau)$. When the number of binding sites is large, substrate predominantly binds to the front of the hub as this is the side initially presented to the surface-bound substrate and very few substrate will be available for binding once the rear of the hub comes within reach. When the number of binding sites is small, substrate binds to more of the hub since the front binding sites are occupied. When the hub is large, the very front of the hub becomes unreachable for substrate to bind.

I also calculated the efficiency of the hub as a function of the hub radius. I found that there was no optimal hub radius that maximized efficiency, rather the efficiency increased as the hub radius decreased. I believe this to be an artifact of the curvature of the hub that positions hub binding sites near the front of the hub further from substrate. Since the hub is unable to roll in this model, the amount of energy able to be delivered to the hub from an extended substrate is limited since the substrate is unable to pull each binding site completely to the equilibrium position.

4.1.4 Summary

These results present possible paths for further research. Additional work could include the possibility of hub rotation or the effect of a R_h on both the diffusion coefficienct and the curvature of the hub. This model could be further fleshed out to provide additional verifiable predictions and further guidance for experimentalists. In other models, much

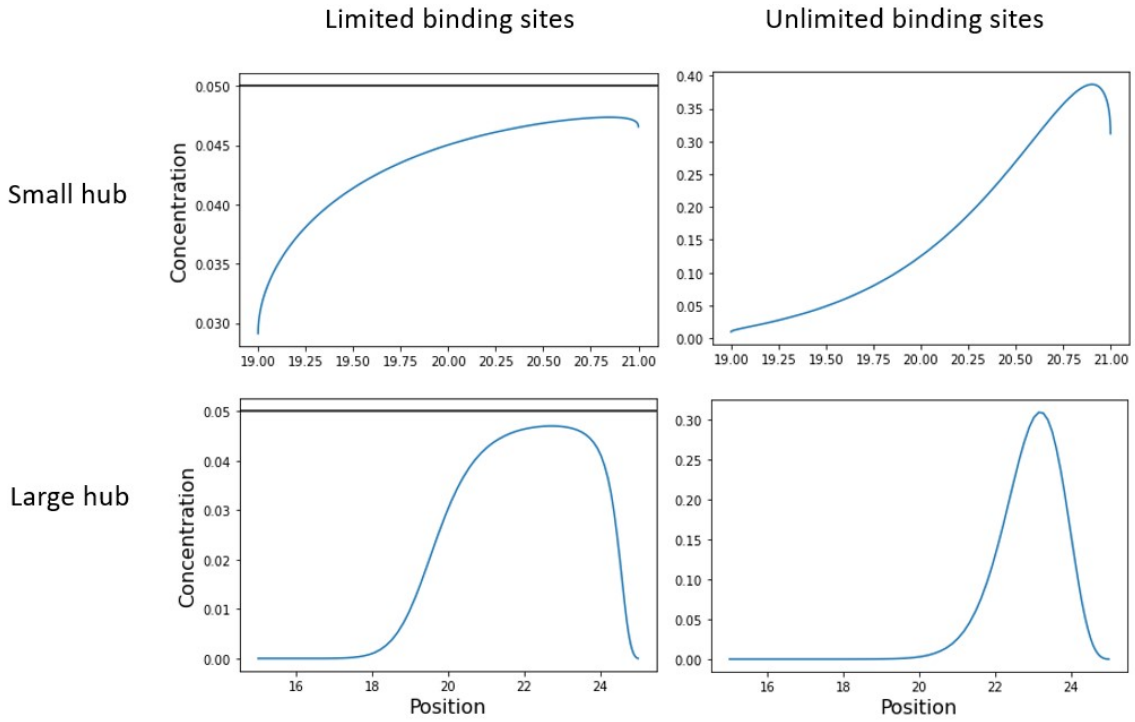

Figure 4.2: **Effect of size and availability on** $B_h(\phi, \tau)$**.** $B_h(\phi, 0) - B_h(\phi, \tau)$ concentration profile for small ($R'_h = 1.0$) and large ($R'_h = 5.0$) hubs and limited ($B_h(\phi, 0) = 0.05$) and less limited binding sites ($B_h(\phi, 0) = 10.0$). The black line represents the maximum number of hub binding sites.

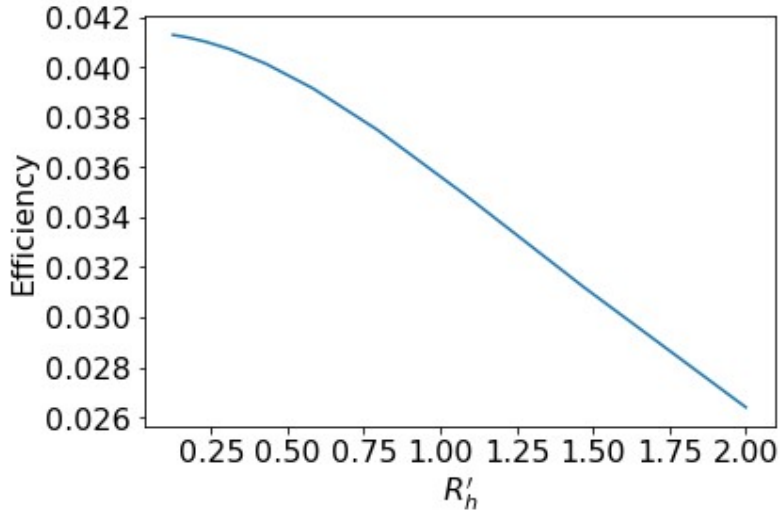

Figure 4.3: **Effect of hub size on efficiency.** Efficiency as a function of hub radius. $\Delta g = 15.0$, $\nu' = 1.0$, $a_{\text{tot}} = 1.0$, $B_h(\phi, 0) = 10.0$.

work has been done in higher dimensions. Extending the model presented in this thesis to interact with a 2D surface could present interesting dynamics. I expect that many system characteristics would be altered. For example, the consumption rate might increase with little increase in velocity due to the possibility of substrate exerting force perpendicular to motion. This perpendicular force might also lead to curvature in the motor's trajectory. I expect the stokes efficiency might still be on a similar order of magnitude since the velocity of the motor would depend on the tangential force from the substrate in a similar manner to our 1D model. It might also be interesting to redefine an effective trajectory, as additional trajectory properties such as persistence length become relevant. Does having a high efficiency lead to an effective motor if the trajectory's persistence length is short? Further discussion around what makes an effective motor could be interesting.

Bibliography

[1] Brian Spear. James Watt: The steam engine and the commercialization of patents. *World patent information*, 30(1):53–58, 2008.

[2] Richard P Feynman. There's plenty of room at the bottom. *Engineering and science*, 23(5), 1959.

[3] Michael Roukes. Nanoelectromechanical systems face the future. *Physics World*, 14(2):25, 2001.

[4] W von Kühne. Eine lebende nematode in einer lebenden muskelfaser beobachtet. *Archiv für pathologische Anatomie und Physiologie und für klinische Medicin*, 26(1):222–224, 1863.

[5] W Engelhardt and M Ljubimowa. Mysoin and adenosinetriphosphatase. *Nature*, 144(1):668–669, 1939.

[6] A Szent-Gyorgyi. Free-energy relations and contraction of actomyosin. *The Biological Bulletin*, 96(2):140–161, 1949.

[7] James A Spudich. The myosin swinging cross-bridge model. *Nature reviews Molecular cell biology*, 2(5):387–392, 2001.

[8] Ian R Gibbons and Arthur J Rowe. Dynein: a protein with adenosine triphosphatase activity from cilia. *Science*, 149(3682):424–426, 1965.

[9] Ronald D Vale, Thomas S Reese, and Michael P Sheetz. Identification of a novel force-generating protein, kinesin, involved in microtubule-based motility. *Cell*, 42(1):39–50, 1985.

[10] T Ross Kelly, Harshani De Silva, and Richard A Silva. Unidirectional rotary motion in a molecular system. *Nature*, 401(6749):150–152, 1999.

[11] Nagatoshi Koumura, Robert WJ Zijlstra, Richard A van Delden, Nobuyuki Harada, and Ben L Feringa. Light-driven monodirectional molecular rotor. *Nature*, 401(6749):152–155, 1999.

[12] Anthony P Davis. Synthetic molecular motors. *Nature*, 401(6749):120–121, 1999.

[13] Maxim N Artyomov, Alexander Yu Morozov, Ekaterina Pronina, and Anatoly B Kolomeisky. Dynamic properties of molecular motors in burnt-bridge models. *Journal of Statistical Mechanics: Theory and Experiment*, 2007(08):P08002, 2007.

[14] T Antal and PL Krapivsky. A" burnt bridge"brownian ratchet. *arXiv preprint cond-mat/0504652*, 2005.

[15] Saveez Saffarian, Ivan E Collier, Barry L Marmer, Elliot L Elson, and Gregory Goldberg. Interstitial collagenase is a brownian ratchet driven by proteolysis of collagen. *Science*, 306(5693):108–111, 2004.

[16] Adam Shellard and Roberto Mayor. Collective durotaxis along a self-generated stiffness gradient in vivo. *Nature*, 600(7890):690–694, 2021.

[17] Tian Jin. Gradient sensing during chemotaxis. *Current opinion in cell biology*, 25(5):532–537, 2013.

[18] James P Zewe, Rachel C Wills, Sahana Sangappa, Brady D Goulden, and Gerald RV Hammond. Sac1 degrades its lipid substrate ptdins4p in the endoplasmic reticulum to maintain a steep chemical gradient with donor membranes. *Elife*, 7:e35588, 2018.

[19] Anthony G Vecchiarelli, Ling Chin Hwang, and Kiyoshi Mizuuchi. Cell-free study of f plasmid partition provides evidence for cargo transport by a diffusion-ratchet mechanism. *Proceedings of the National Academy of Sciences*, 110(15):E1390–E1397, 2013.

[20] Anthony G Vecchiarelli, Yong-Woon Han, Xin Tan, Michiyo Mizuuchi, Rodolfo Ghirlando, Christian Biertümpfel, Barbara E Funnell, and Kiyoshi Mizuuchi. Atp control of dynamic p1 para–dna interactions: a key role for the nucleoid in plasmid partition. *Molecular microbiology*, 78(1):78–91, 2010.

[21] Anthony G Vecchiarelli, Kiyoshi Mizuuchi, and Barbara E Funnell. Surfing biological surfaces: exploiting the nucleoid for partition and transport in bacteria. *Molecular microbiology*, 86(3):513–523, 2012.

[22] Alisina Bazrafshan, Maria-Eleni Kyriazi, Brandon Alexander Holt, Wenxiao Deng, Selma Piranej, Hanquan Su, Yuesong Hu, Afaf H El-Sagheer, Tom Brown, Gabriel A Kwong, et al. Dna gold nanoparticle motors demonstrate processive motion with bursts of speed up to 50 nm per second. *ACS nano*, 15(5):8427–8438, 2021.

[23] Lavisha Jindal and Eldon Emberly. Dna segregation under par protein control. *Plos one*, 14(7):e0218520, 2019.

[24] Aaron T Blanchard. Burnt bridge ratchet motor force scales linearly with polyvalency: a computational study. *Soft Matter*, 17(25):6056–6062, 2021.

[25] Laleh Samii, Heiner Linke, Martin J Zuckermann, and Nancy R Forde. Biased motion and molecular motor properties of bipedal spiders. *Physical Review E*, 81(2):021106, 2010.

[26] Falko Ziebert and Igor M Kulić. How influenza's spike motor works. *Physical Review Letters*, 126(21):218101, 2021.

[27] Shoichi Toyabe and Eiro Muneyuki. Experimental thermodynamics of single molecular motor. *Biophysics*, 9:91–98, 2013.

[28] Salma Kassem, Thomas van Leeuwen, Anouk S Lubbe, Miriam R Wilson, Ben L Feringa, and David A Leigh. Artificial molecular motors. *Chemical Society Reviews*, 46(9):2592–2621, 2017.

[29] Ronald D Vale. Millennial musings on molecular motors. *Trends in Genetics*, 15(12):M38–M42, 1999.

[30] Hideo Higuchi and Sharyn A Endow. Directionality and processivity of molecular motors. *Current opinion in cell biology*, 14(1):50–57, 2002.

[31] Anatoly B Kolomeisky and Michael E Fisher. Molecular motors: a theorist's perspective. *Annual review of physical chemistry*, 58(1):675–695, 2007.

[32] Erdal Toprak, Ahmet Yildiz, Melinda Tonks Hoffman, Steven S Rosenfeld, and Paul R Selvin. Why kinesin is so processive. *Proceedings of the National Academy of Sciences*, 106(31):12717–12722, 2009.

[33] Jeffrey T Finer, Robert M Simmons, and James A Spudich. Single myosin molecule mechanics: piconewton forces and nanometre steps. *Nature*, 368(6467):113–119, 1994.

[34] T Ross Kelly, Imanol Tellitu, and Jose Perez Sestelo. In search of molecular ratchets. *Communications*, 36(107):1866–1867, 1997.

[35] Günther Woehlke and Manfred Schliwa. Directional motility of kinesin motor proteins. *Biochimica et Biophysica Acta (BBA)-Molecular Cell Research*, 1496(1):117–127, 2000.

[36] Sinan Can, Samuel Lacey, Mert Gur, Andrew P Carter, and Ahmet Yildiz. Directionality of dynein is controlled by the angle and length of its stalk. *Nature*, 566(7744):407–410, 2019.

[37] Peter R Ashton, Roberto Ballardini, Vincenzo Balzani, Ian Baxter, Alberto Credi, Matthew CT Fyfe, Maria Teresa Gandolfi, Marcos Gómez-López, M-Victoria Martínez-Díaz, Arianna Piersanti, et al. Acid- base controllable molecular shuttles. *Journal of the American Chemical Society*, 120(46):11932–11942, 1998.

[38] Renjun Pei, Steven K Taylor, Darko Stefanovic, Sergei Rudchenko, Tiffany E Mitchell, and Milan N Stojanovic. Behavior of polycatalytic assemblies in a substrate-displaying matrix. *Journal of the American Chemical Society*, 128(39):12693–12699, 2006.

[39] Beatrice Ramm, Andriy Goychuk, Alena Khmelinskaia, Philipp Blumhardt, Hiromune Eto, Kristina A Ganzinger, Erwin Frey, and Petra Schwille. A diffusiophoretic mechanism for atp-driven transport without motor proteins. *Nature Physics*, 17(7):850–858, 2021.

[40] Koen Visscher, Mark J Schnitzer, and Steven M Block. Single kinesin molecules studied with a molecular force clamp. *Nature*, 400(6740):184–189, 1999.

[41] Benjamin H Blehm, Trina A Schroer, Kathleen M Trybus, Yann R Chemla, and Paul R Selvin. In vivo optical trapping indicates kinesin's stall force is reduced by dynein during intracellular transport. *Proceedings of the National Academy of Sciences*, 110(9):3381–3386, 2013.

[42] Roop Mallik, Dmitri Petrov, SA Lex, SJ King, and SP Gross. Building complexity: an in vitro study of cytoplasmic dynein with in vivo implications. *Current Biology*, 15(23):2075–2085, 2005.

[43] Aaron T Blanchard, Alisina S Bazrafshan, Jacob Yi, Julia T Eisman, Kevin M Yehl, Teng Bian, Andrew Mugler, and Khalid Salaita. Highly polyvalent dna motors generate 100+ pn of force via autochemophoresis. *Nano letters*, 19(10):6977–6986, 2019.

[44] Philip Nelson. *Biological physics*. WH Freeman New York, 2004.

[45] Christopher Jarzynski. Equalities and inequalities: Irreversibility and the second law of thermodynamics at the nanoscale. *Time*, pages 145–172, 2013.

[46] Oliver Pänke and Bernd Rumberg. Energy and entropy balance of atp synthesis. *Biochimica et Biophysica Acta (BBA)-Bioenergetics*, 1322(2-3):183–194, 1997.

[47] Nazul Jared López Alamilla and Ivan Santamaría Holek. Reconstructing the free-energy landscape associated to molecular motors processivity. *Biophysical Chemistry*, 167:16–25, 2012.

[48] Kei-ichi Okazaki and Shoji Takada. Dynamic energy landscape view of coupled binding and protein conformational change: induced-fit versus population-shift mechanisms. *Proceedings of the National Academy of Sciences*, 105(32):11182–11187, 2008.

[49] Barbara J Gabryś, Karol Pesz, and Stanisław J Bartkiewicz. Brownian motion, molecular motors and ratchets. *Physica A: Statistical Mechanics and its Applications*, 336(1-2):112–122, 2004.

[50] Toshio Yanagida, Masahiro Ueda, Tsutomu Murata, Seiji Esaki, and Yoshiharu Ishii. Brownian motion, fluctuation and life. *Biosystems*, 88(3):228–242, 2007.

[51] Henry Riall Sankey. The thermal efficiency of steam-engines.(including appendixes). In *Minutes of the Proceedings of the Institution of Civil Engineers*, volume 125, pages 182–212. Thomas Telford-ICE Virtual Library, 1896.

[52] Karel Proesmans and Christian Van den Broeck. Stochastic efficiency: five case studies. *New Journal of Physics*, 17(6):065004, 2015.

[53] Gatien Verley, Massimiliano Esposito, Tim Willaert, and Christian Van den Broeck. The unlikely carnot efficiency. *Nature communications*, 5(1):1–5, 2014.

[54] Hongyun Wang and G Oster. The stokes efficiency for molecular motors and its applications. *EPL (Europhysics Letters)*, 57(1):134, 2002.

[55] Alan J Hunt, Frederick Gittes, and Jonathon Howard. The force exerted by a single kinesin molecule against a viscous load. *Biophysical journal*, 67(2):766–781, 1994.

[56] Karel Svoboda and Steven M Block. Force and velocity measured for single kinesin molecules. *Cell*, 77(5):773–784, 1994.

[57] Kenji Kawaguchi and Shin'ichi Ishiwata. Temperature dependence of force, velocity, and processivity of single kinesin molecules. *Biochemical and biophysical research communications*, 272(3):895–899, 2000.

[58] George Banting, Steve J Higgins, Kazuhiko Kinosita, Ryohei Yasuda, and Hiroyuki Noji. F1-atpase: a highly efficient rotary atp machine. *Essays in Biochemistry*, 35:3–18, 2000.

[59] Ryohei Yasuda, Hiroyuki Noji, Kazuhiko Kinosita Jr, and Masasuke Yoshida. F1-atpase is a highly efficient molecular motor that rotates with discrete 120 steps. *Cell*, 93(7):1117–1124, 1998.

[60] S Rice, Y Cui, C Sindelar, N Naber, M Matuska, R Vale, and Roger Cooke. Thermodynamic properties of the kinesin neck-region docking to the catalytic core. *Biophysical Journal*, 84(3):1844–1854, 2003.

[61] Yuhan Huang, Nic C Surawski, Yuan Zhuang, John L Zhou, and Guang Hong. Dual injection: An effective and efficient technology to use renewable fuels in spark ignition engines. *Renewable and Sustainable Energy Reviews*, 143:110921, 2021.

[62] Leon Brillouin. Maxwell's demon cannot operate: Information and entropy. i. *Journal of Applied Physics*, 22(3):334–337, 1951.

[63] Andrew Rex. Maxwell's demon—a historical review. *Entropy*, 19(6):240, 2017.

[64] Ignacio A Martinez, Édgar Roldán, Luis Dinis, and Raúl A Rica. Colloidal heat engines: a review. *Soft matter*, 13(1):22–36, 2017.

[65] Charles H Bennett. Notes on landauer's principle, reversible computation, and maxwell's demon. *Studies In History and Philosophy of Science Part B: Studies In History and Philosophy of Modern Physics*, 34(3):501–510, 2003.

[66] Aniruddha Mitra, Marc Suñé, Stefan Diez, José M Sancho, David Oriola, and Jaume Casademunt. A brownian ratchet model explains the biased sidestepping of single-headed kinesin-3 kif1a. *Biophysical journal*, 116(12):2266–2274, 2019.

[67] R Dean Astumian and Imre Derényi. A chemically reversible brownian motor: application to kinesin and ncd. *Biophysical journal*, 77(2):993–1002, 1999.

[68] Akihiko Nakamura, Kei-ichi Okazaki, Tadaomi Furuta, Minoru Sakurai, and Ryota Iino. Processive chitinase is brownian monorail operated by fast catalysis after peeling rail from crystalline chitin. *Nature communications*, 9(1):1–12, 2018.

[69] Jordan M Horowitz and Massimiliano Esposito. Thermodynamics with continuous information flow. *Physical Review X*, 4(3):031015, 2014.

[70] Tushar K Saha, Joseph NE Lucero, Jannik Ehrich, David A Sivak, and John Bechhoefer. Bayesian information engine that optimally exploits noisy measurements. *arXiv preprint arXiv:2204.07310*, 2022.

[71] Patrick T Underhill and Patrick S Doyle. Development of bead-spring polymer models using the constant extension ensemble. *Journal of Rheology*, 49(5):963–987, 2005.

[72] Max von Delius and David A Leigh. Walking molecules. *Chemical Society Reviews*, 40(7):3656–3676, 2011.

[73] Rachid Ait-Haddou and Walter Herzog. Brownian ratchet models of molecular motors. *Cell biochemistry and biophysics*, 38(2):191–213, 2003.

[74] Chapin S Korosec and Nancy R Forde. The lawnmower: an artificial protein-based burnt-bridge molecular motor. *arXiv preprint arXiv:2109.10293*, 2021.

[75] Ivan E Collier, Wesley Legant, Barry Marmer, Olga Lubman, Saveez Saffarian, Tetsuro Wakatsuki, Elliot Elson, and Gregory I Goldberg. Diffusion of mmps on the surface of collagen fibrils: the mobile cell surface–collagen substratum interface. *PloS one*, 6(9):e24029, 2011.

[76] Linghao Zhong, James F Matthews, Michael F Crowley, Tauna Rignall, César Talón, Joseph M Cleary, Ross C Walker, Giridhar Chukkapalli, Clare McCabe, Mark R Nimlos, et al. Interactions of the complete cellobiohydrolase i from trichodera reesei with microcrystalline cellulose iβ. *Cellulose*, 15(2):261–273, 2008.

[77] Xiongce Zhao, Tauna R Rignall, Clare McCabe, William S Adney, and Michael E Himmel. Molecular simulation evidence for processive motion of trichoderma reesei cel7a during cellulose depolymerization. *Chemical Physics Letters*, 460(1-3):284–288, 2008.

[78] Christina L Ting, Dmitrii E Makarov, and Zhen-Gang Wang. A kinetic model for the enzymatic action of cellulase. *The journal of physical chemistry B*, 113(14):4970–4977, 2009.

[79] Chun Geun Lee, Carla A Da Silva, Charles S Dela Cruz, Farida Ahangari, Bing Ma, Min-Jong Kang, Chuan-Hua He, Seyedtaghi Takyar, and Jack A Elias. Role of chitin and chitinase/chitinase-like proteins in inflammation, tissue remodeling, and injury. *Annual review of physiology*, 73, 2011.

[80] Yasuyuki Arakane and Subbaratnam Muthukrishnan. Insect chitinase and chitinase-like proteins. *Cellular and molecular life sciences*, 67(2):201–216, 2010.

[81] Kei-ichi Okazaki, Akihiko Nakamura, and Ryota Iino. Chemical-state-dependent free energy profile from single-molecule trajectories of biomolecular motors: Application to processive chitinase. *The Journal of Physical Chemistry B*, 124(30):6475–6487, 2020.

[82] K Okazaki, A Nakamura, and R Iino. Dynamic free energy landscape of a linear motor chitinase from single-particle tracking trajectories. *bioRxiv*, page 655878, 2019.

[83] Pierre A Devijver. Baum's forward-backward algorithm revisited. *Pattern Recognition Letters*, 3(6):369–373, 1985.

[84] Ling Chin Hwang, Anthony G Vecchiarelli, Yong-Woon Han, Michiyo Mizuuchi, Yoshie Harada, Barbara E Funnell, and Kiyoshi Mizuuchi. Para-mediated plasmid partition driven by protein pattern self-organization. *The EMBO journal*, 32(9):1238–1249, 2013.

[85] Jakob Møller-Jensen, Jonas Borch, Mette Dam, Rasmus B Jensen, Peter Roepstorff, and Kenn Gerdes. Bacterial mitosis: Parm of plasmid r1 moves plasmid dna by an actin-like insertional polymerization mechanism. *Molecular cell*, 12(6):1477–1487, 2003.

[86] Adam C Brooks and Ling Chin Hwang. Reconstitutions of plasmid partition systems and their mechanisms. *Plasmid*, 91:37–41, 2017.

[87] Anjana Badrinarayanan, Tung BK Le, and Michael T Laub. Bacterial chromosome organization and segregation. *Annual review of cell and developmental biology*, 31:171, 2015.

[88] Lavisha Jindal and Eldon Emberly. Operational principles for the dynamics of the in vitro para-parb system. *PLoS computational biology*, 11(12):e1004651, 2015.

[89] Longhua Hu, Anthony G Vecchiarelli, Kiyoshi Mizuuchi, Keir C Neuman, and Jian Liu. Brownian ratchet mechanism for faithful segregation of low-copy-number plasmids. *Biophysical journal*, 112(7):1489–1502, 2017.

[90] Longhua Hu, Anthony G Vecchiarelli, Kiyoshi Mizuuchi, Keir C Neuman, and Jian Liu. Brownian ratchet mechanisms of para-mediated partitioning. *Plasmid*, 92:12, 2017.

[91] Swarup Dey, Chunhai Fan, Kurt V Gothelf, Jiang Li, Chenxiang Lin, Longfei Liu, Na Liu, Minke AD Nijenhuis, Barbara Saccà, Friedrich C Simmel, et al. Dna origami. *Nature Reviews Methods Primers*, 1(1):1–24, 2021.

[92] Tosan Omabegho, Ruojie Sha, and Nadrian C Seeman. A bipedal dna brownian motor with coordinated legs. *science*, 324(5923):67–71, 2009.

[93] William B Sherman and Nadrian C Seeman. A precisely controlled dna biped walking device. *Nano letters*, 4(7):1203–1207, 2004.

[94] Jong-Shik Shin and Niles A Pierce. A synthetic dna walker for molecular transport. *Journal of the American Chemical Society*, 126(35):10834–10835, 2004.

[95] Mark Rempel and Eldon Emberly. Optimizing efficiency and motility of a polyvalent molecular motor. *Micromachines*, 13(6):914, 2022.

[96] Avin Ramaiya, Basudev Roy, Michael Bugiel, and Erik Schäffer. Kinesin rotates unidirectionally and generates torque while walking on microtubules. *Proceedings of the National Academy of Sciences*, 114(41):10894–10899, 2017.

[97] Michio Tomishige, Nico Stuurman, and Ronald D Vale. Single-molecule observations of neck linker conformational changes in the kinesin motor protein. *Nature structural & molecular biology*, 13(10):887–894, 2006.

[98] A Alexander-Katz and RR Netz. Surface-enhanced unfolding of collapsed polymers in shear flow. *EPL (Europhysics Letters)*, 80(1):18001, 2007.

[99] Charles S Epstein and Ariana J Mann. Measurement of the dna spring constant using optical tweezers. *Phys. Rev. E*, 67:051906, 2003.

[100] Lü Ming-Tao, Yan Ming-Yue, Ai Bao-Quan, Gao Tian-Fu, and Zheng Zhi-Gang. Stokes efficiency in the overdamped brownian ratchet. *ACTA PHYSICA SINICA*, 66(22), 2017.

[101] Anthony G Vecchiarelli, Keir C Neuman, and Kiyoshi Mizuuchi. A propagating atpase gradient drives transport of surface-confined cellular cargo. *Proceedings of the National Academy of Sciences*, 111(13):4880–4885, 2014.

[102] Malcolm P Kennett. *Essential Statistical Physics*. Cambridge University Press, 2020.

[103] Ralf Metzler and Joseph Klafter. The random walk's guide to anomalous diffusion: a fractional dynamics approach. *Physics reports*, 339(1):1–77, 2000.

[104] Johan OL Andreasson, Bojan Milic, Geng-Yuan Chen, Nicholas R Guydosh, William O Hancock, and Steven M Block. Examining kinesin processivity within a general gating framework. *Elife*, 4:e07403, 2015.